FINITE ELEMENT ANALYSIS OF CORRODED RC BEAMS

A Thesis Submitted in the partial Fulfillment of the Requirement for the Award of the Degree of

MASTER OF ENGINEERING

in Structure

Submitted By

Meet Sompura

801724014

Under Supervision of

Dr. Naveen Kwatra
Professor

Dr. Trishna Choudhury
Assistant Professor

DEPARTMENT OF CIVIL ENGINEERING

THAPAR INSTITUTE OF ENGINEERING AND TECHNOLOGY,

PATIALA- 147004, (INDIA).

JULY-2019

DECLARATION

I, Meet Sompura hereby declare that the work presented in this thesis entitled "**FINITE ELEMENT ANALYSIS OF CORRODED RC BEAMS**" in the partial fulfillment of the requirement for the award of degree of Master of Engineering Structural Engineering submitted at the Civil Engineering Department, Thapar Institute of Engineering & Technology (Deemed to be University), Patiala is an authentic record of work carried out by me under the supervision of Dr. Naveen Kwatra, Professor and Dr. Trishna Choudhury Assistant Professor, Department of Civil Engineering, T.I.E.T. Patiala. The matter presented in this has not been submitted either in part or full to any other university or institute for the award of any other degree.

Date: 12/8/19

Meet Sompura
Roll No.-801724014

This is to certify that above declaration made by the student concerned is correct to the best of my knowledge and belief.

Dr. Naveen Kwatra
Professor,
Department of Civil Engineering,
T.I.E.T., Patiala-147004

Dr. Trishna Choudhury
Assistant professor,
Department of Civil Engineering,
T.I.E.T., Patiala-147004

Date: 12/8/19

ii

ACKNOWLEDGEMENT

First and foremost, I would like to express my sincere gratitude to my guide Dr. Naveen Kwatra, Professor and Dr. Trishna Choudhury, Assistant Professor Department of Civil Engineering for their gracious efforts and esteem guidance throughout the course of this work. Their keen interest and continuous support led to the successful completion of this research work.

I would like to thank all the faculty members of Department of Civil Engineering, T.I.E.T. Patiala for their assistance in the research work. Thank you.

Meet Sompura

M.E. (Structures)

Roll no.- 801724014

ABSTRACT

Reinforcement corrosion has been remained one of the primary environmental factors responsible for RC structure degradation. Rebar corrosion significantly affect the service life of an RC structure. The maintenance and repair work policy should be proactive to restrict corrosion induced damage at optimum cost. Hence it becomes very important to understand the effect of corrosion in an RC beam. A paramount importance has been given to damage assessment of a corroded RC beam. Various experimental investigation has carried out to study the performance of an RC beam due to rebar corrosion. However, the limitations involved with experimental investigations restrict us from having the complete picture of corrosion studies.

A 3D nonlinear finite element analysis is an effective tool to simulate the effect of rebar corrosion in an RC beam. A finite element model allows to incorporate various boundary conditions and loading conditions for the corroded RC beam.

A comprehensive 3D nonlinear finite element model has proposed for the corroded RC beams. It includes all the primary effects due to rebar corrosion 1) Bond strength degradation, 2) spalling stresses on concrete and 3) Area reduction of the rebar. Finite element model is validated with experimental results. Multiple finite element analysis has performed to find out the effect of rebar corrosion at a constant sustainable load on the RC beam. An optimum maintenance point has proposed to obtain the optimum maintenance and repair work cost for the corroded RC beam. Spalling stress variations has observed with increase of bending stress in a corroded RC beam. An effort has been made to relate the spalling stress variation with global behaviour of the corroded RC beam.

TABLE OF CONTENT

LIST OF TABLES

LIST OF FIGURES

CHAPTER-1

INTRODUCTION

1.1 OVERVIEW

Reinforced concrete has been one of the widely used construction material around the world since the 19th century. Reinforce concrete (RC) has been used extensively for almost all construction projects like buildings, bridges, dams etc. Growing usage of reinforced concrete material for construction illustrates it's benefits like economical, easy availability, durability, stability and strength. However, RC structures deteriorate in extreme situations, such as marine environment, exposure to deicing salt and high concentration of chloride/carbon dioxide atmosphere. Eventually these environmental conditions resulted into corrosion on the reinforcement. Rebar corrosion in an RC beam gradually degrades the structural performance of the RC beam. The rebar corrosion in an RC beam is expected to decrease its ultimate strength and deflection.

Therefore, it becomes necessary to maintain and monitor the structural health of RC structures, an effective maintenance and repair work strategy for any RC structures and to uphold a suitable work strategy in case the RC beam is exposed to rebar corrosion. Moreover, the structural maintenance and repair work for RC beams subjected to corrosion induces substantial cost. Hence it is essential to determine the damage due to rebar corrosion. It allows to improve the service life of RC structures with the help of proactive measures.

The present work discusses and illustrates numerical modelling related to the corrosion of RC beams, its effects, modelling strategy, and improvement over past studies carried out in the past. Thrust has also been laid on the response of the corroded RC beams under serviceability loads which directly represents the practical scenario in a building. The bond strength degradation along with the spalling stress have successfully implemented in a 3D finite element model for corroded RC beam.

1.2 QUANTIFICATION OF THE DAMAGE DUE TO CORROSION

The qualitative effects of rebar corrosion in RC beams are well known by experimental investigation. However, it would require a quantitative assessment of the corroded RC

beam to provide aid in maintenance and safety measurements. The following are the reasons to quantify the corrosion-induced damage in an RC beam.

1) It helps us to understand the damage mechanism of rebar corrosion.
2) To capture the behaviour of a corroded RC beam under damaged condition.
3) In order to determine the degradation due to corrosion in terms of load carrying capacity and ultimate deflection of an RC beam.
4) To determine the residual service life of the structure.
5) To draft a cost-effective maintenance and repair work policy for any RC structure which is experiencing corrosion attack.
6) In order to predict the threshold limit for rebar corrosion in an RC beam.
7) It enables to study failure mechanism more precisely.
8) To establish the relation between local effects due to corrosion and their global effect on the performance of a corroded RC beam.

1.3 CORROSION AND ITS EFFECT ON THE RC BEAM

Concrete is an alkaline medium in which steel reinforcement are arranged to improve its tension carrying capacity. Steel reinforcement-bar consists of iron as a major part of the substance. Therefore, iron atoms are likely to form corrosion product once they exposed to chloride ion and oxide in the presence of water. The alkalinity of the concrete material protects the reinforcement from chloride ion and carbon dioxide penetration to the rebar surface. However, the alkalinity of the concrete material does not remain intact over a long period of time. This time period specifically termed as depassivation of concrete material. Once the concrete is depassivated, chloride ions and carbon dioxide start to reach rebar surface and initiate the corrosion.

Practical examples of RC structures deteriorating due to corrosion are very well depicted by (Kamaitis, 2011). In 1992, Switzerland, three bridges were demolished due to substantial corrosion damage(Kamaitis, 2011). Experiments have been performed to understand the response of corroded RC beams(Rodriguez *et al.,* 1997; Lee *et al.*, 1999). All of them had observed that rebar corrosion in an RC beam significantly reduces the load carrying capacity as well as the ultimate deflection of the RC beam. Corrosion in the reinforcement alters the failure mechanism of the RC beam. Increase of corrosion leads to sudden failure of an RC beam.

The bond strength degradation between steel and concrete, loss of cross-sectional area of reinforcement and loss of concrete integrity are the primary factors responsible behind the corrosion-induced damage in an RC beam(Lee *et al.*, 1999; Coronelli and Gambarova, 2004). In order to quantify the damage due to corrosion, the responsible factors must be examined carefully at various level of corrosion.

1.4 IMPORTANCE OF FINITE ELEMENT MODEL

Finite element (FE) analysis is an effective numerical technique available to solve the partial differential equations. Various engineering problems consist of material nonlinearity and geometrical nonlinearity are efficiently solved by nonlinear finite element analysis. Although it is an approximate analysis method it gives fairly accurate results based on the importance of the finite element model. The main advantages of the FE analysis over experimental studies are low cost and less time-consuming option, less manpower requirement, the flexibility of performing parametric study and multiple simulations using various boundary conditions. Finite element analysis allows to examine the local stress and strain variation at each node of the model which may not be convenient through experimentation. The local stress variations will help in understanding the overall global response of the model. However, numerical results must be validated with experimental results before any parametric study of RC beams.

The FE analysis of corroded RC beams has been a topic of study over a long period of time. Several researchers have proposed their finite element models to include the rebar corrosion effects in various ways. However, limited attention has been given on a development of comprehensive FE model based on the brief literature survey. Not much emphasis has been given on the development of the 3D finite element model which include bond strength degradation and spalling stress due to corrosion. Hence a comprehensive finite element model has proposed to explore the detail understanding of the rebar corrosion. A 3D nonlinear FE model is developed which includes the bond strength degradation and spalling stresses due to volume increase with respect to level of corrosion in longitudinal bars of RC beam.

1.5 OBJECTIVE

The pivotal objective of this work is to present a comprehensive finite element model for corroded RC beams. The Finite element model should be able to represent the bond strength degradation, loss of effective cross-section area of the rebar and concrete spalling to

represent the corrosion-induced damage in an RC beam. In order to incorporate the bond strength degradation with an increase in corrosion level, a bond slip model between reinforcement and concrete surface should be modelled correctly.

Experimentally, a specific level of corrosion is induced in RC beams before actually loaded in the testing frame. However, in the real conditions of an RC beam the rebar corrosion and exposure to service load goes on simultaneously. Therefore, the effect of corrosion at sustainable loading on the RC beam has been studied.

The salient objectives of the present work are listed below.

1) To develop a 3D nonlinear FE model for corroded RC beam including spalling stresses at rebar concrete interface and bond strength degradation.
2) To observe the effect of corrosion under sustainable loading on an RC beam for different level of corrosion.
3) To establish a relation between the local effects due to corrosion at rebar level and its contribution at a global behaviour of corroded RC beams.

1.6 SCOPE OF THE WORK

A 3D FE model is developed in the Abaqus software including the bond slip behaviour of rebar and concrete and the spalling stress on the concrete at different level of corrosion. The results of the numerical analysis have validated with experimental works in form of load-deflection curve. Two beams of size 200 x 250 x 2000mm and 150 x 200 x 2000 mm has modelled for the analysis. The bottom bars of each beams are uniformly corroded to 3.8%, 7.9% & 25.3% and 13.88%, 17.2% and 13.88%, 17.2% & 26.04% respectively. The incorporation of bond-slip model is checked by comparing the load deflection curve with perfectly bonded condition of concrete and reinforcement, as well as experimental results for the control specimen. Finite element analysis has performed for each corroded RC beam specimen. With an increase of the level of corrosion in the rebars corrosion in an RC beam, a reduction in the load carrying and the ultimate deflection has been observed.

The validated finite element models further used for multiple analysis with various level of corrosion in the reinforcement. The load-deflection curve of each corroded beam model helps to understand the effect of corrosion under sustainable loading on the RC beam. Variation in the deflection with an increase of corrosion of the RC beam had observed at design load.

Spalling stress variations with an increase of the bending stress in the RC beam has determined. Spalling stresses at various location along the length of the RC beam has observed at cracking load, yield load and ultimate load.

1.7 OUTLINE OF THE THESIS

The present study broadly addresses the numerical the numerical analysis of RC beams considering the effects of rebar corrosion. Emphasis has been laid on including all the detrimental effects of corrosion, that include induction of spalling stresses, degradation in the bond strength, change in the area and volume of rebars due to corrosion. The work carried out is organized as follows.

Chapter-1: Introduction to the topic in general, basic need and objective of the present study.

Chapter-2: Discussion of the previous studies carried out on study of corrosion in RC beams. Various techniques adopted for FE analysis of corroded RC beams.

Chapter-3: Technique for the finite element modelling of corroded RC beams in the ABAQUS software.

Chapter-4: Discusses the results of numerical study carried out, validation with past studies and spalling stress variation with bending stress of an RC beam.

Chapter-5: Conclusion and future scope.

CHAPTER-2

LITERATURE REVIEW

2.1 OVERVIEW

Corrosion is the primary factor that significantly affect the service life of an RC beam. Effects of corrosion must be considered in order to obtain the actual service life of an RC beam. Therefore, it would be necessary to understand the corrosion process, its propagation and effects in the RC beam. This chapter consist of research work related to corrosion progression, effects of corrosion and their formulation in an RC beam. Research work related to FE model of corroded RC beam has depicted in this chapter to understand modelling difficulties and gap of literature.

2.2 CORROSION MECHANISM

Reinforced concrete (RC) structures experience a gradual deterioration due to various environmental factors. Among these factors, rebar corrosion is the most influential factor that affects the durability of RC structures. Since the responsible elements that induce the corrosion on rebars are oxygen and chloride ions, the rebar corrosion can be categorized as carbonation corrosion and chloride ingress corrosion respectively. The alkaline nature of concrete, it prevents the oxide and chloride ion penetration from the outer environment to rebars. Once the concrete loses its alkaline nature corrosion process initiates on the rebars. The carbonation corrosion produces uniform corrosion products around the rebars, known as rust, whereas the chloride corrosion leads to pitting or localised corrosion(Committee on the safety of nuclear Installations, 2002). Rust products inhabit a higher volume compared to the same amount of reinforcing steel material since it is primarily responsible for cover cracking of concrete. Nonetheless, the chloride induced corrosion reduce the cross-section of reinforcement locally along the length of rebar. Consequences of the rebar corrosion in RC structures can be very well understood by Figure-2.1.

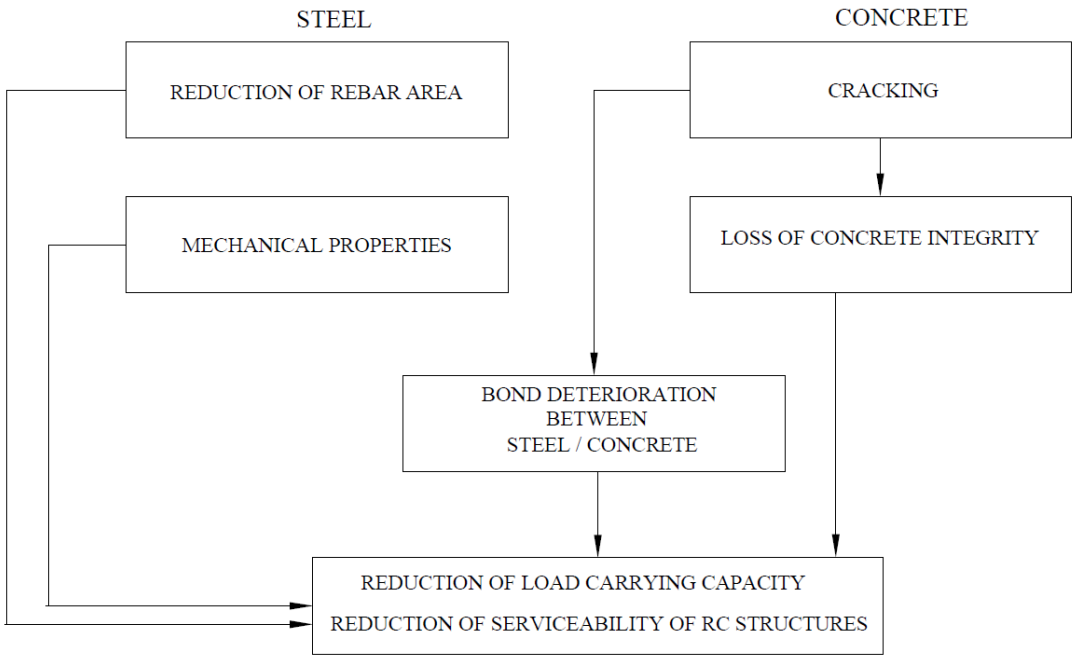

Figure-2.1 – Consequences of corrosion on structural performance (Committee on the safety of nuclear Installations, 2002)

Various researchers(Rodriguez *et al.,* 1997; Lee *et al.*, 1999; Maaddawy *et al.*,2005) have studied the effect of corrosion on the RC beams through experimental investigation. Different level of corrosion technique was achieved through accelerated corrosion technique to study the effect of rebar corrosion on RC beams. The expected level of corrosion was achieved using the Faraday's law, which predicts mass loss due to corrosion based on corrosion current and time of applying current in the rebars. The loss of mass due to accelerated corrosion has predicted using Faraday's law as in Equation (2.1).

$$\Delta m_s = \frac{I_{corr} \times T \times M}{Z \times F} \tag{2.1}$$

$$I_{corr} = i_{corr} \times (\pi d_b l) \tag{2.2}$$

Δm_s = Mass loss (g)

I_{corr} = Current (A)

T = time (sec) required for Δm_s mass loss

M = atomic mass of steel (56 g for Fe)

F = Faraday's constant (96500 As)

Z = ionic charge (Fe^{2+})

i_{corr} = current density (A/m^2)

d_b = diameter of steel bar

l = length of steel bar

RC beams used to test after a specific time period of passing current in the reinforcement bars. The weight loss of corroded bars measured after loading test to obtain the exact percentage of corrosion. There are various non-destructive techniques available to monitor the reinforcement corrosion in an RC beam. Reinforcement corrosion in an actual RC beam is monitored by non-destructive testing (NDT) methods such as X-ray, acoustic emission, radiography, ultrasonic guided waves. Among all these methods ultrasonic guided waves is a promising one to measure the amount of corrosion in reinforcement of real RC structures(Sharma and Mukherjee, 2011).

The basic effects of rebar corrosion in the various materials used in RC structures are listed by Lee *et al.*,(2002) and Coronelli and Gambarova (2004) as 1) bond strength degradation at rebar concrete interface 2) Reduction in cross-sectional area of reinforcement and 3) Loss of concrete integrity due to loss of cover cracking and concrete spalling. Each of these are discussed in detail in the next section.

2.3 EFFECTS OF REBAR CORROSION ON RC BEAMS

As there are mainly 3 consequences of rebar corrosion, bond strength degradation, loss of area of the rebar, cover cracking of concrete or concrete spalling.

2.3.1 Bond strength degradation

Various researchers (Cabrera, 1996; Lee *et al.,* 2002; Chung *et al.,* 2004; Bhargava *et al.*, 2007; Jiang *et al.,* 2018) have studied the bond strength evolution with an increase of rebar corrosion. Bond strength degradation with an increase of corrosion has been measured experimentally from pullout tests.

Cabrera (1996) studied the effect of corrosion on the loss of bond strength experimentally. Further he proposed a bond strength degradation model with respect to the level of corrosion. It was stated that the fundamental problem associated with corrosion-induced damage is not the loss of strength of reinforcement bars, but it is the stress exerted within the concrete by the corrosion products. This internal stress reduces concrete strength as

well as the bond strength between concrete and steel. This degradation of bond strength due to rebar corrosion significantly affects the serviceability and load carrying capacity of RC members. Cabrera, (1996) conducted pullout tests and flexure tests to determine the bond strength variation and deflection variation respectively due to corrosion. The main drawback of bond strength degradation model Cabrera (1996) is that it does not consider the increase of bond strength in the initial level 2% of corrosion. This usually results in an overestimation of bond strength degradation at an initial level of corrosion. Also, the beam test specimen used for conducting the experiments did not consider any lateral ties.

Similar pullout tests of the reinforced concrete specimen were carried out by Lee *et al.*,(2002) and the results were checked against the results of FE analysis. It was concluded that the RC beam specimen with no lateral reinforcement experienced brittle failure due to corrosion while the specimens with lateral ties fail by slipping of rebar due to confinement effect. FEM analysis results of the pullout test also complied with experimental results. The drawback of (Lee, Noguchi and Tomosawa, 2002) model is ignoring the increase of bond strength at the initial level of corrosion.

Bhargava *et al.*, (2007) and Bhargava *et al.*, (2008) extensively studied the bond strength degradation on corroded RC beams through experimental investigation and proposed an analytical model as well as an empirical model. The empirical model relates the bond strength to percentage of corrosion based on experimental results. Since it has been observed in experiments that initially up to around 2% of corrosion, the bond strength increases and then after starting to decline. This relationship of bond strength to the level of corrosion also consider using a holistic approach. The bond strength remains constant up to a corrosion level of 1.5% to avoid overestimation of bond strength reduction as proposed in the empirical model of Bhargava *et al.*, (2008).. Although the empirical model proposed is for RC beams without stirrups, but it can be applied for RC beams with stirrups. The relation between bond strength and level of corrosion proposed based on pullout tests and flexural tests are shown in Eq. (2.3) to (2.6).

a) Based on pullout tests

$$R = 1 \qquad X_p \leq 1.5\% \tag{2.3}$$

$$R = 1.192 \times e^{-0.117X_p} \quad X_p > 1.5\% \tag{2.4}$$

b) Based on flexural tests data

$$R = 1 \qquad X_p \leq 1.5\% \tag{2.5}$$

$$R = 1.346 \times e^{-0.198X_p} \quad X_p > 1.5\% \tag{2.6}$$

R = bond strength (MPa)

X_p = % of corrosion

Bhargava *et al.*, (2007) explained the behaviour of corroded RC beams failing in bond. Bond failure at the interface between steel concrete responsible for failure of corroded RC beams. The bond between concrete and reinforcement deteriorates to such an extent that further increase of load, resulting in the concentrated stresses at the anchorage ends of reinforcement. Therefore, the load carrying capacity of corroded beams also influences by anchorage length of reinforcement before the bond failure of corroded beam. The above empirical model shows a good correlation with experimental data. The variation between experimental and empirically predicted values may be attributed to Variation of material properties, the electrical properties of concrete, the composition of reinforcing bar.

Jiang, *et al.*, (2018) combined various experimental data of previous research and performed regression analysis. The bond slip model proposed by Jiang, *et al.*, (2018) consists of important factors which influence the bond slip behaviour. The whole bond slip curve evolves with the change of corrosion level in the proposed model. Effect of concrete spalling and confinement effect due to stirrups had been included in the bond slip behaviour in form of variables by Jiang, *et al.*, (2018). Bond slip behaviour of Jiang, *et al.*, (2018) has implemented in the FE model for modelling the corrosion in an RC beam.

2.3.2 Area loss of the rebars

Percentage of corrosion directly relate to the reduction in cross sectional area of reinforcement. However, the implementation of this effect in the FE model can be done using two different approaches:- 1) by reducing the area of the cross-section for the corroded bar based on the level of corrosion(Dekoster *et al.*, 2003; Coronelli and Gambarova, 2004; Biondini and Vergani, 2014) or 2) by reducing the yield strength, elastic modulus and ultimate strength of rebar based on the level of corrosion. (Lee *et al.*, 1999).

2.3.3 Cover cracking of concrete or concrete spalling

Concrete spalling and cover cracking due to corrosion is an important phenomenon as it affects the loss of concrete integrity (Yu *et al.*, 2015) and initiates the bond strength

degradation(Bhargava *et al.*, 2007). Since rust products of corrosion occupy volume about 6-10 times higher of the same amount of steel material (Broomfield , 2007), this volume expansion leads to concrete spalling and delamination of concrete cover. (Bhargava *et al.*, 2007) proposed an empirical model for bond degradation in which bond strength starts decreasing after 1.5% of corrosion. The initiation of the reduction of bond strength attributed to spalling stresses and loss of concrete integrity. Cover cracking of concrete initiates after hoop tensile stress increase above the initial tensile strength of concrete(f_{ct}). Maaddawy and Soudki, (2007) stated that the cover cracking of concrete due to corrosion marks the end of its functional service life after that repair would be necessary for structure. Due to its paramount influence on such things, it becomes crucial to model the corrosion induced hoop tensile stress at concrete and reinforcement interface precisely. Bazant (1979) proposed an analytical model to forecast the time period from corrosion initiation to cover cracking of RC beams. It considers that the time period from corrosion initiation to cover cracking mainly depends on corrosion rate, cover depth, spacing between rebar, the size of reinforcement and properties of concrete. It assumes that all the uniform corrosion (rust) responsible for hoop tensile stress induced at the steel-concrete interface. Bazant (1979) did not validate his model with experimental results. Later Liu and Wayers (1998) extended the research work of Bazant (1979) and reported that there is a porous layer exist at the interfacial zone of concrete and steel that allows corrosion to expand freely without generating any hoop tensile stresses. Liu and Wayers (1998) additionally, also consider the free expansion time of corrosion due to the porous layer. The size of the porous layer depends upon the size of reinforcement, the volume of rust and steel concrete interface. As steel-concrete interface influenced by various factors like w/c ratio, aggregate size, degree of consolidation and hydration etc. Consideration of the porous layer at steel-concrete interface shows good agreement with experimental outcomes for time to corrosion cracking model. Liu and Wayers (1998) had also validated their model with experimental results of 5 years of outdoor exposure of slab. Liu and Wayers (1998) assumed that the corrosion induced rate of mass loss of steel decreases as time progress. As this assumption underestimates the mass loss of rebar compared to the value obtained by Faraday's law. Since the predicted mass loss of steel using Faraday's law display a good agreement with experimentally measured values(Maaddawy and Soudki, 2003). Maaddawy and Soudki, (2007) proposed a modified analytical model to predict the internal radial pressure and time period of corrosion initiation to cover cracking. It considered the effect of free expansion of corrosion due to the porous layer around rebar as well as the mass loss of rebar according

to Faraday's law. The thickness of the porous layer ranges between 10 to 20 μm (El Maaddawy and Soudki, 2007).

Few researchers have incorporated the effect of concrete spalling in FE analysis of corroded RC beams(Dekoster *et al.*, 2003; Coronelli and Gambarova, 2004; Biondini and Vergani, 2014). Dekoster *et al.*,(2003) had considered the overall effect of bond strength degradation and concrete spalling in the form of rust element. A material property of rust element like modulus of elasticity reduces with the increase of corrosion. Coronelli and Gambarova, (2004) included concrete spalling effect separately from bond strength degradation. Coronelli and Gambarova, (2004) proposed a technique to reduce the compressive strength of concrete element near cover region. The compressive strength reduces with the increase of corrosion level to represent the damage due to concrete spalling. Ožbolt *et al.,* (2011) conducted a crack propagation study due to corrosion cross-sectionally. However, at present a model considering both the load and corrosion induced cracking together is not available (Otieno,*et al.,* 2011).

2.4 FE ANALYSIS OF CORRODED RC BEAM

Researchers have studied various methodology to include the effects of corrosion in the FE analysis of corroded RC beams. The advantages and drawbacks of the same will be discussed in this section.

Lee *et al.*, (1999) performed experimental as well as FE analysis on the corroded RC beam. The experimental work consists of four RC beam, out of which one controlled RC beam (BS) and other three RC beams were corroded at 3.8%(BCD-1), 7.9%(BCD-2) and 25.9%(BCD-3) of uniform corrosion. The tension reinforcement bars were corroded using electrolytic corrosion method. A direct current of 1A applied on each specimen for the specific time period. To determine the % of corrosion, the weight loss of rebars measured after removing the rust from rebars. Corrosion particles on rebar remove using diammonium hydrogen citrate to measure weight loss. Four-point bending test was performed on the RC beams. Results are represented in Figure-2.2 in terms of a load-displacement graph.

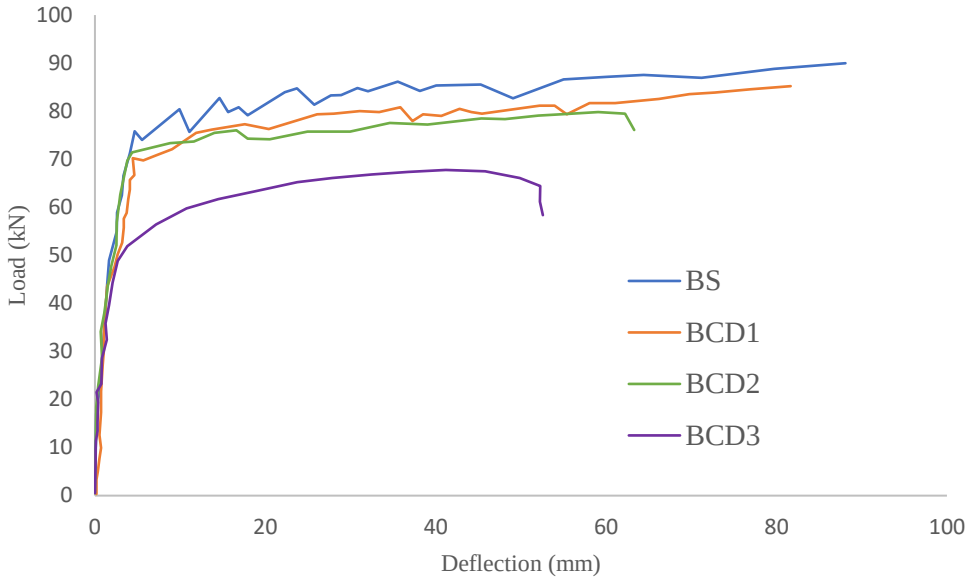

Figure-2.2 Load – Deflection curves(Lee *et al.*, 1999)

Lee *et al.*, (1999) performed the finite element analysis of the same experimental specimen. The material model for concrete considered as an isotropic material. The input data of the compressive strength, tensile strength and poisons ratio used to define concrete material, obtained from experiments. Finite element analysis of RC beam performed considering concrete as 4 node isoparametric plane stress element and steel rebars as 2 node truss elements.

Link elements defined between steel and concrete element to model bond slip behaviour in the FE model of RC beams. The effects of corrosion considered in the form of reducing the yield strength of steel bars and bond strength degradation between concrete and steel bars. Model for Bond strength and yield strength reduction with % of corrosion derived empirically from the experimental data. (Lee *et al.*, 1999) proposed the equations for reducing bond strength and yield strength with the increase of corrosion as Eq. (2.7) to (2.11)

Yield strength (σ_{cy}):

Uniform corrosion $\sigma_{cy} = \left(1 - 1.24\left(\frac{\delta w}{100}\right)\right) \times \sigma_{sy}$ (2.7)

Pitting corrosion $\sigma_{cy} = \left(1 - 1.98\left(\frac{\delta w}{100}\right)\right) \times \sigma_{sy}$ (2.8)

Elastic modulus (E_{cs}):

Uniform and pitting corrosion $E_{cs} = \left(1 - 1.24\left(\frac{\delta w}{100}\right)\right) \times E_{ss}$ (2.9)

$\tau_{max} = 5.21 \times e^{-0.0561\Delta w}$ (2.10)

$D_s = 1160 \times \Delta w^{-1.014}$ (2.11)

Where σ_{sy} = yield strength of sound rebar, σ_{cy} = yield strength of corroded rebar, δw = percentage of corrosion, E_{cs} = elastic modulus for corroded rebar, E_{ss} = elastic modulus for sound rebar. τ_{max} = bond strength (MPa), Δw = % of corrosion and D_s = bond rigidity (MPa).

Figure.-2.3a and 2.3b shows the load deflection curve obtained from FE analysis of (Lee *et al.*, 1999).

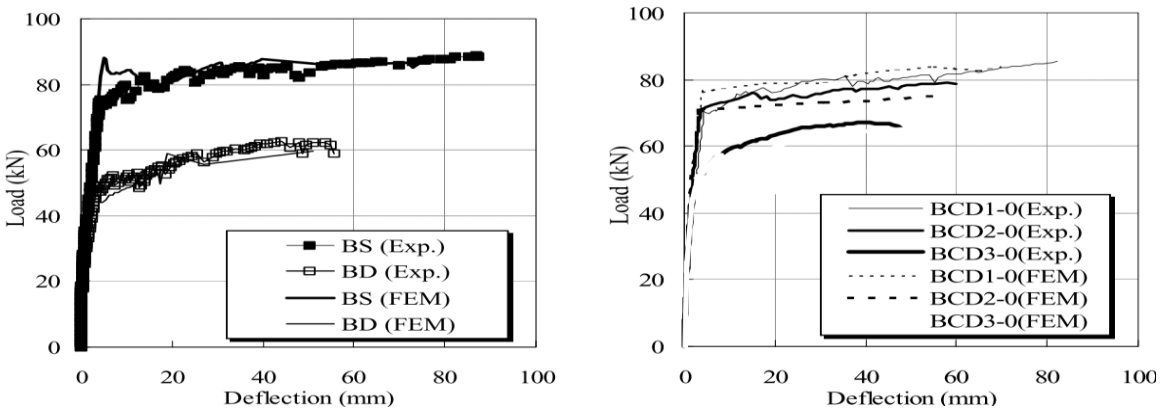

(a) **(b)**

Figure.2.3 Load-deflection curve of FE analysis(Lee *et al.*, 1999)

A 2D finite element model has an advantage of low computational efforts compared to 3D models. However, the assumption for concrete elements as a plane stress element may not remain valid for practical conditions. As this assumption would be applicable only if the ends of the beam are free(Otieno *et al.*, 2011). FE model of Lee *et al.*, (1999) does not consider the corrosion-induced cracking in the concrete, as it happens in the real structures in the form of spalling of concrete.

Dekoster *et al.*, (2003) performed FE analysis of corroded RC beams and validated their results with experimental work of the Lee *et al.*, (1999). Two different types of material model considered for concrete material, 1) elastic plastic approach 2) damage approach. Steel reinforcement modelled, considering an elastic-plastic stress-strain relationship with isotropic work hardening. 2D finite element analysis had been performed using CASTEM 2000 software, assuming concrete elements as plane stress elements. 3 node triangular elements had used for concrete while 2 node linear bar elements had used for reinforcement.

In elastic plastic approach (EPA) the failure surface in compression and tension defined as per Drucker-Prager and Rankine yield criteria respectively. In damage approach (DA) the effect of failure is incorporated by modifying the Young's modulus with the help of damage variable D.

The parameters responsible for representing the corrosion effect in the FE model are following 1) reduction in cross-section area 2) bond strength degradation.

Bond strength degradation was incorporated with the help of modelling rust elements at the interface between rebar and concrete. 3 node triangular elements were selected as rust elements which serve as a volumetric element based on percentage of corrosion. Rust elements have specific material property. To link the real condition with plan stress condition, the author expressed the modulus of elasticity and section property into equivalent parameters as written in Eq. (2.12) and (2.13)

Real section of rust (S_r) = $8\pi r^2(1 - \sqrt{1-\eta})$ (2.12)

Equivalent section of rust (s_r) = $2re\ (1 - \sqrt{1-\eta})$

Modulus of elasticity $E_r = 3(1- 2\nu_r)\ K_r$ (2.13)

Equivalent modulus $E_{eqr} = E_r \frac{Sr}{sr}$

ν_r = Poissons ratio (0.49)

K_r = Bulk modulus (2 GPa)

r = radius of rebar

η = % of corrosion

e = width of the beam

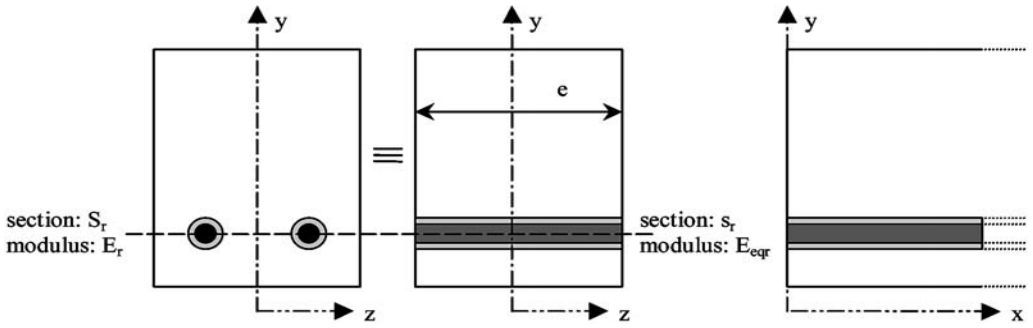

Figure.-2.4 Real and fictitious rust section(Dekoster *et al.*, 2003)

The results from finite element analysis using elastic plastic approach and damage approach are as shown in Figure- 2.5a and 2.5b respectively. As it can be seen that damage approach is more reliable to predict the load deflection behaviour of corroded RC beams.

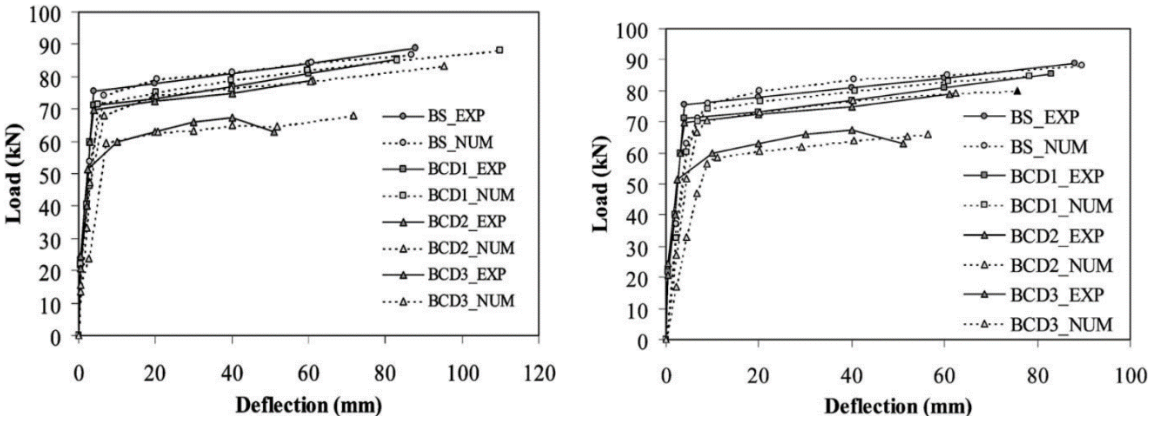

(a) **(b)**

Figure-2.5 Load-Deflection curve (a) EPA test (b) DA test

Finite element analysis carried out by (Dekoster *et al.*, 2003) has similar drawbacks when it compared with the FE model of the (Lee *et al.*, 1999). Although the elastic plastic approach and damage approach for concrete material did not capture the correct behaviour of quasi-brittle material, they were reliable technique compared to the material model of (Lee *et al.*, 1999). It has to be noted that none of these two approaches alone is able to represent the nonlinear response of concrete(Alfarah *et al.*, 2017). Plastic models do not consider the stiffness degradation observed in experiments (Grassl and Jirásek, 2006). The damaged based model is not able to capture irreversible deformations and inelastic volumetric expansion in compression.

(Coronelli & Gambarova, 2004) carried out FE analysis of corroded RC beams followed by validation with experimental results of (Rodriguez *et al.*, 1997). (Coronelli &

Gambarova, 2004) had performed 2D finite element analysis assuming concrete as 4 node plane stress elements. Rebars modelled as 2 node truss elements. Incremental stress-stain relation with smeared rotating cracks considered for concrete. Equivalent tensile strength had used to avoid mesh dependency. Biaxial failure surface was used to define the strength of the material.

The effects of corrosion in finite element analysis mainly incorporated with the help of reducing the bond strength at the steel-concrete interface, compressive strength of concrete and ultimate strain of steel rebars. Bond slip model between steel and concrete implemented using the link elements. Bond stress vs slip behaviour modified based on corrosion attack penetration. The bond model used here was proposed by (Rodriguez et al., 1994). Limitation of this bond model is that it can be applicable for medium size bars only. since regression analysis carried out for limited experimental data. Compressive strength of concrete elements at cover of a RC beam reduced to include the effect of concrete spalling(Coronelli and Gambarova, 2004). (Coronelli and Gambarova, 2004) performed 2D FE analysis of corroded RC beam. Figure-2.6 presents the FE model of corroded RC beams.

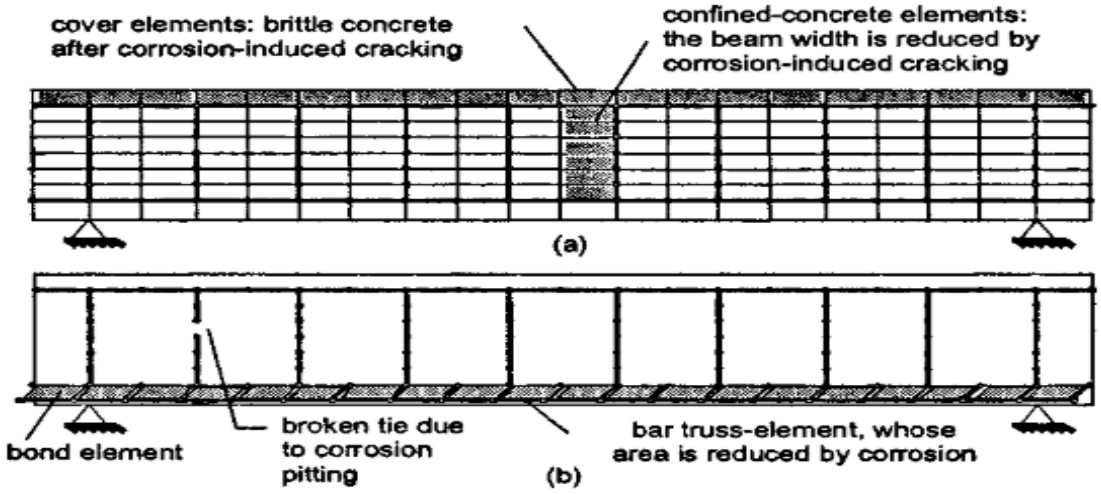

Figure-2.6 Finite element model of corroded RC beam(Coronelli and Gambarova, 2004)

FE results were validated with experimental work of (Rodriguez *et al.*, 1997). The beam 11.1 is a control RC beam whereas 11.4, 11.5 and 11.6 are corroded RC beam. Although finite element analysis results are in reasonable agreement with experimental work, the methodology of FE analysis requires calibration each time before any practical implementation. As the inclusion of spalling stress through reduction of compressive

strength of concrete at the cover region is remain an empirical approach. The yield strength of rebars assumed as 575 Mpa for all the bars in the elastic-plastic model. In experimental work of (Rodriguez, Ortega and Casal, 1997) it was reported different for each diameter of the reinforcement. 2D finite element analysis remains valid for certain boundary condition only where ends of RC beam are free.

(Biondini and Vergani, 2014) performed 3D nonlinear FE analysis of corroded RC beams. It was verified with experimental results of Rodriguez *et al.*,(1997). Corrosion effects in the finite element analysis were incorporated by a reduction in the cross-section area of rebar, the ultimate strain of steel and the compressive strength of concrete. Loss of compressive strength of concrete at cover element represents the damage due to spalling stress. Model used to predict reduction in compressive strength due to spalling stress is same as proposed in Coronelli and Gambarova, (2004). The damage in the concrete cover as represented by a reduced compressive strength of concrete elements at cover region is shown in Figure-2.7.

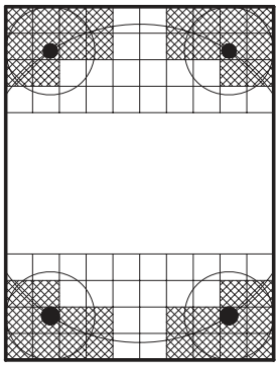

Figure.2.7 Damaged elements of concrete (Biondini and Vergani, 2014)

The results of FE analysis of (Biondini and Vergani, 2014) are as shown in Figure-2.8. Bond strength degradation did not include as an effect of corrosion in the FE model. An empirical model for a reduction in an ultimate strain of steel also limited to a specific set of experiment. Although reduction of compressive strength of concrete elements at cover region provides good match with experimental results, acceptability and limitations of this technique is not very well defined for larger set of experimental data.

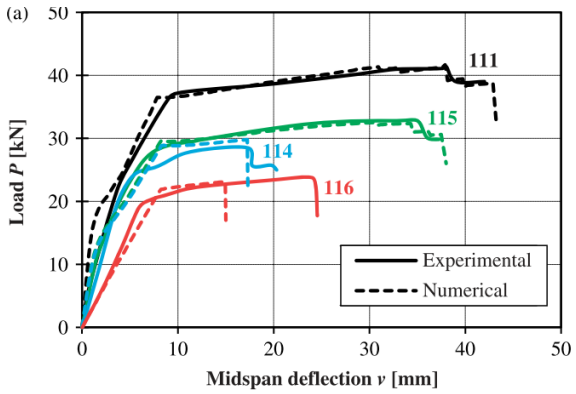

Figure-2.8 Load-deflection curve (Biondini and Vergani, 2014)

2.5 NEED FOR RESEARCH

The present chapter discusses the work carried out by various researchers in the past to develop techniques for the FE analysis of corroded RC beams through the timeline. So far, much emphasis has been put on the 2D FE analysis of corroded RC beams and it has evolved and improved over the period of time. The 2D finite element models are relatively simple and computationally efficient compared to 3D FE models. However, the 2D models have predefined assumptions that limit its applicability within a practical scenario. In the 2D finite element model of RC beams, concrete elements are assumed as plane stress element along the width of the beam, but this assumption is valid only until both ends of an RC beam are free. Another downside is that the confinement effect of stirrups on the concrete is modeled by an increase in the compressive strength of concrete using empirical relation. In addition, the effect of torsion is also challenging to analyse with a 2D model of RC beams. These limitations can be overcome by adopting a 3D FE model of corroded RC beam.

Bond strength degradation would be an essential component for any FE model of corroded RC beam, since the bond between the concrete and steel is greatly affected by the corrosion of rebars. Till date, the bond - slip behaviour between rebar and concrete has been implemented in 2D analysis only. There is a very limited literature available which has implemented bond - slip behaviour on a 3D-FE model of an RC beam.

Inclusion of spalling stresses in the numerical model remains an unexplored aspect of FE analysis of corroded RC beams. The damage due to spalling stresses is mostly represented through reduction of compressive strength of concrete elements at the cover region. which is more of an empirical approach. and does not relate well with the actual condition of concrete spalling. Therefore, a comprehensive finite element (FE) model is required for

corroded RC beam, which includes all these effects due to corrosion and moreover it should be flexible for any boundary conditions.

The present study, considers a 3D nonlinear finite element model for modelling corroded RC beams that can captures the impact of corrosion reliably and overcome the drawbacks of previously developed models. The adopted model relates well to the actual scenario of corrosion in RC beam.

CHAPTER-3

FE MODEL OF A CORRODED RC BEAM

3.1 OVERVIEW

The main purpose of the present research work is to develop a comprehensive FE model for corroded RC beams. A 3D nonlinear FE model is developed to predict the corrosion induced damage in RC beams. FE analysis is performed using the software package Abaqus. A 3D bond model between concrete and steel surfaces has been incorporated to capture the effect of rebar corrosion in RC beam. Spalling stresses due to corrosion has been included successfully to observe local variations of stresses due to rebar corrosion. The model is able to provide localised information about bond stress variation and spalling stresses at reinforcement level along with overall behaviour of the RC beam. Two different sets of experimental results were verified with the help of finite element method. Overall, nineteen RC beam models are analysed using Abaqus to verify and study the various detrimental effects of corrosion in RC beams. Nonlinear static analysis iss performed for each finite element model for various level of corrosion.

3.2 FINITE ELEMENT MODEL OF AN RC BEAM

For RC beams in the present study, two different modelling approaches have been carried out. Firstly, the longitudinal reinforcement bars are assumed to be perfectly bonded with concrete, whereas in the second approach the interaction between rebars and the concrete is defined by a bond slip model. Each of the finite element modelling approach needs data consisting of reinforcement detailing, concrete proportion and loading plates. The detail of the bond model is discussed later in the chapter.

Longitudinal reinforcements of an RC beam are modelled as 3D elements in finite element analysis. These 3D elements of the rebars are essential in order to incorporate bond model and spalling stresses in the finite element model. 1D beam elements considered to model the shear reinforcement in the finite element model. Concrete material modelled as 8 node 3D brick element, while loading plate considered as a rigid plate of 4 node 2D element.

In the perfectly bonded finite element model reinforcement of an RC beam model as an embedded region inside of the concrete material. A hole of rebar diameter size requires to

create through concrete material to incorporate the bond slip behaviour between steel and concrete interface. Rebar part must fit into the hole of concrete material such that rebar surface and concrete surface keep in touch with each other. Bond properties can be defined between concrete and rebar surfaces using cohesive surface or cohesive element approach.

3.3 MATERIAL MODEL

Material model for concrete and reinforcement is an important input parameter for any nonlinear analysis subjected to material nonlinearity. Each of these are discussed in detail in the subsequent paragraphs.

3.3.1 Concrete

Two material models are available to define nonlinearity of concrete material in the Abaqus. 1) concrete damage plasticity model 2) concrete smeared cracking. Concrete smeared cracking model is developed to model the monotonic loading response of the concrete material. Whereas concrete damaged plasticity model is able to model the response effectively under cyclic loading. Keeping in mind the future scope of the research work, concrete damaged plasticity model is implemented for concrete material.

The concrete damage plasticity model considers mainly two failure mechanism for concrete 1) cracking in tension and 2) crushing in compression. The yield surface and failure surface are governed by two hardening variables ε_c^{pl} and ε_t^{pl} respectively. Where ε_c^{pl} and ε_t^{pl} are plastic strain in compression and tension respectively. Five parameters require to specify before defining uniaxial stress train curve in compression and tension (Abaqus manual).

1) Dilation angle (Ψ)

Dilation angle is a variable require to define the flow potential function. The flow potential function represents the volume change caused due to plastic distortions for concrete material (Lubliner J. et al.1989). Most accepted value of the dilation angle for concrete material is 31^0.

2) Eccentricity

Eccentricity defined as the rate of plastic potential function approaches to the asymptote in the p-q plane. p is the hydrostatic stress component and q is the deviatoric stress component. The value of eccentricity for concrete is considered as 0.1. Figure-3.1 explains the dilation angle and eccentricity very well.

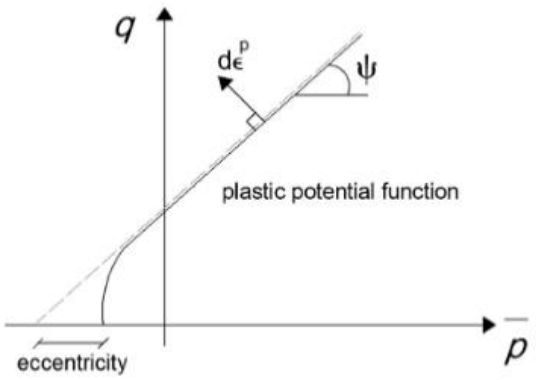

Figure-3.1 Dilation angle and eccentricity in meridian plane (Abaqus Manual, 2014)

3) Fb_0/fc_0

Ratio of initial equibiaxial compressive yield stress to the initial uniaxial compressive yield stress (Abaqus Analysis User's manual). The default value used to consider for concrete as 1.16.

4) K

It is the ratio of second stress invariant on the tensile meridian to that on the compressive meridian. The value of K ranges from 0.5 to 1. While 0.5 and 1 value of K describe Rankine yield surface and Drucker-Prager yield surface respectively on the deviatoric stress plane. It is generally taken as 2/3 as shown in Figure-3.2.

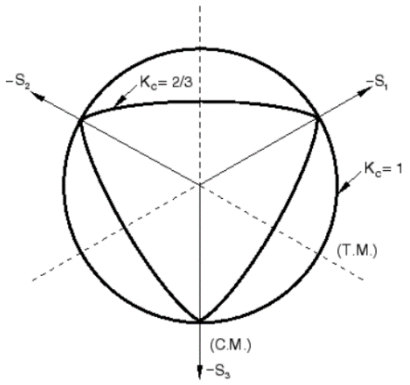

Figure-3.2 Yield surface in deviatoric plane (Abaqus manual, 2014)

5) Viscosity parameter

Material model exhibiting the nonlinearity often lead to convergence problem in implicit analysis. To avoid some of these convergence difficulties viscosity parameter used to define in the material model. The value for viscosity parameter considered as 0.00001 through all the finite element analysis.

3.3.1.1 Concrete in compression

Stress strain curve of concrete in compression mainly divide into three segments 1) linear elastic curve (0 - $0.4f_{ck}$) 2) elastic-plastic curve ($0.4f_{ck}$ – f_{ck}) 3) softening curve (f_{ck} – 0). Figure-3.3 shows the schematic diagram of stress strain curve for concrete in compression and the stress strain curve implemented in the finite element analysis for compression behaviour of the concrete.

1) Linear elastic curve

Initial elastic curve of concrete generated through elastic property of material section in the ABAQUS. It is assumed that concrete in compression remain elastic up to stress of $0.4f_{ck}$. modulus of elasticity was considered as per equation (3.1) and poisson's ratio assumed to be 0.2 for concrete.

$$E_0 = 4700 \times \sqrt{f_{ck}} \tag{3.1}$$

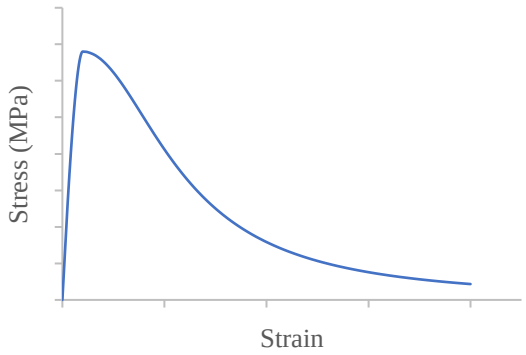

Figure- 3.3 Stress-strain curve of concrete in compression

2) Elastic-plastic curve

The ascending region of elastic plastic curve ranges from $0.4f_{ck}$ – f_{ck} on the stress axis. The stress strain curve for elastic plastic region considered as per (CEB-FIP, 2010). The following Eq. (3.2) represent the elastic plastic curve for concrete in compression.

$$\sigma_c = f_c \left(\frac{k.\eta - \eta^2}{1+(k-2).\eta}\right) \tag{3.2}$$

$$\eta = \frac{\varepsilon}{\varepsilon_c} \;\; \& \;\; k = \frac{E_0}{E_C}$$

σ_c = Compressive stress of concrete (MPa)

f_c = Compressive strength of concrete (MPa)

η = normalised strain

ε = strain

ε_c = strain at peak stress f_c

E_0 = initial elastic modulus (MPa)

E_c = secant elastic modulus at peak stress = $f_c/\ \varepsilon_c$ (MPa)

3) Softening curve of concrete in compression

The softening curve of concrete in compression determined as per Equation (3.3) (Alfarah *et al.*, 2017). It is noticed that softening curve of concrete in compression dependent on the size of finite element selected for analysis.

$$\sigma_c = \left(\frac{2+(\gamma_c f_c \varepsilon_c)}{2f_c} - \gamma_c \varepsilon_c + \frac{\varepsilon_c^2 \gamma_c}{2\varepsilon_c}\right)^{-1} \quad (3.3)$$

$$\gamma_c = \frac{\pi^2 f_c \varepsilon_c}{2\left(\frac{G_{ch}}{l_{eq}} - 0.5 f_c\left(\varepsilon_c(1-b) + b\frac{f_c}{E_0}\right)\right)^2} \quad , \text{b} = \frac{\varepsilon_c^{pl}}{\varepsilon_c^{ch}}$$

G_{ch} = Crushing energy per unit area (N/mm)

l_{eq} = characteristic length of an element

b = 0.9 assumed based on experimental observations(Alfarah, *et al.*, 2017)

Crushing energy value determined from the following set of equation (3.4) & (3.5).

$$G_f = 0.073 f_c^{0.18} \quad (3.4)$$

$$G_{ch} = \left(\frac{f_c}{f_t}\right)^2 G_f \quad (3.5)$$

$$f_t = 0.3016(f_c)^{2/3} \quad (3.6)$$

G_f = fracture energy per unit area (N/mm)

f_t = tensile strength of concrete (MPa)

3.3.1.2 Concrete in tension

Relation between stress and crack width for concrete in tension was calculated based on Eq.(3.7) (Hordijk DA. 1992). The displacement control method is selected in Abaqus software to incorporate the input data in form of stress displacement variables.

$$\sigma_t = f_t \left[\left(1 + \left(\frac{c_1 W}{W_c} \right)^3 \right) e^{-c_2 \frac{W}{W_c}} - \frac{W}{W_c} (1 + c_1^3) e^{-c_2} \right] \quad (3.7)$$

Fracture crack opening (W_c) = 0.3 mm

c_1 = 3 & c_2 = 6.93 (Hordijk DA, 1992)

Generally, W_c value assumed as per Eq.(3.3.8)(CEB-FIP, 2010) which ranges between 0.1 mm to 0.3 mm. A higher value of W_c = 0.3 mm has assumed in the Eq. (3.7) to include tension stiffening effect in the concrete material model. Therefore, Stress value does not reach to zero value corresponding to actual value of W_c. The stress-crack width curve is defined the plastic property of concrete material in tension as shown in Figure-3.4.

$$W_c = \frac{5.14 G_f}{f_t} \quad (3.8)$$

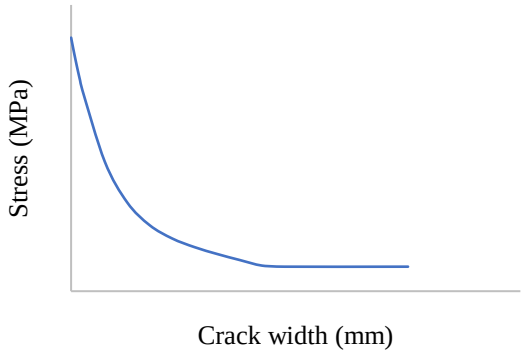

Figure-3.4 Stress-crack width curve of concrete in tension

3.3.2 Material model for reinforcement

Material model for steel reinforcement mainly influences the plastic behaviour of an RC beam and ultimate deflection of the beam. An elastic-plastic model along with strain hardening had been used for steel reinforcement of an RC beam. In order to predict the ultimate deflection of an RC beam, stress strain curve after ultimate stress had defined as a decline in the stress. Figure- 3.5 shows the stress strain curve of steel reinforcement include in the FE analysis. The actual values of modulus of elasticity, F_y and F_u were used as per reported in the experimental data for finite element analysis. Because of no experimental data is available on the ultimate strain (ε_u) value of a rebar. Ultimate strain (ε_u) value adjusted such that finite element results have the same or near value of ultimate deflection compared to experimental data.

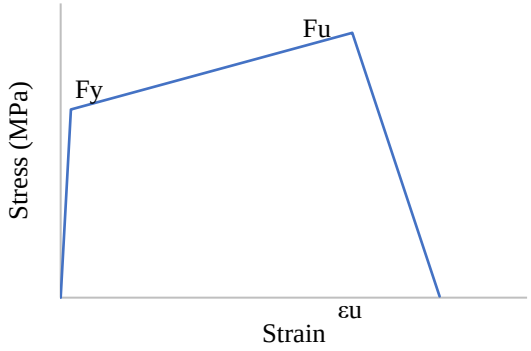

Figure-3.5 Stress strain curve for reinforcement

3.4 REBAR CORROSION EFFECT IN FE MODEL

It is well known fact that rebar corrosion adversely affects any RC beams from the available literature. The following mechanism causes the damage in an RC beam due to rebar corrosion.

1) Bond strength degradation
2) Concrete spalling & cover cracking
3) Area reduction of a rebar

It becomes important to implement the effect of rebar corrosion with a appropriate technique in the finite element model to predict the accurate and reliable results. The effects of rebar corrosion are implemented briefly in the FE model. The finite element model is able to provide the insight about local behaviour of a corroded RC beam such as spalling stress variation and bond stress variation. To capture bond strength degradation due to corrosion had implemented in the finite element analysis. Concrete spalling effect included as the outward normal pressure on the concrete surface at the rebar concrete interface. The following subsections briefly describes the implementation methods of corrosion induced damage in the Abaqus software.

3.4.1 Bond slip behaviour

Bond strength degradation is an important effect of corrosion induced damage on RC beam. Therefore, it would be necessary to include bond strength degradation in the FE model of corroded RC beam for reliability of the analysis. Bond model had defined in the initial step of the finite element analysis. Abaqus software check the bond model defined in the initial step to ensure that the two surfaces are in touch with each other or separated. Bond model behaviour incorporated between the surfaces which remain in touch with each other. Bond

model has been implemented successfully between the rebar and concrete surface in a 3D finite element model.

A bond-slip behaviour proposed by Jiang et al., (2018) has been implemented to model bond strength degradation due to rebar corrosion. The proposed bond slip behaviour for various level of corrosion consists of the following set of Eq. (3.9) to (3.15).

$$\tau_n = \frac{(\tau_{max})_n}{\left[e^{-Bln(\frac{B}{D})/(B-D)} - e^{-Dln(\frac{B}{D})/(B-D)}\right]}(e^{BS} - e^{DS}) \quad (3.9)$$

$$(\tau_{max})_n = \frac{2.5(\sqrt{f_c})_n}{1+3.1e^{-0.47[(K_{co})_n+33K_{st}]}} \quad (3.10)$$

$$\left(\sqrt{f_c}\right)_n = \sqrt{f_c}[0.5 + 0.5cos(n^{0.514}\pi)] \quad (3.11)$$

$$(K_{co})_n = \frac{c}{d_b}\frac{1-n}{1-27.027n+1099.275n^2} \quad (3.12)$$

$$K_{st} = \frac{A_{st}}{nS_{st}d_b} \quad (3.13)$$

$$B = \frac{0.0254+K_{st}}{-0.0232-8.34K_{st}} \quad (3.14)$$

$$D = 3\ ln\left(\frac{0.7315+(K_{co})_n+33K_{st}}{5.176+0.333[(K_{co})_n+33K_{st}]} - 0.13\right) - 3.375 \quad (3.15)$$

τ_n = Bond stress (MPa)

S = Slip (mm)

$(\tau_{max})_n$ = Maximum bond stress (MPa)

n = % corrosion on a rebar

f_c = Compressive strength of concrete (MPa)

c = Clear cover (mm)

d_b = Diameter of longitudinal bar (mm)

A_{st} = Area of stirrups (mm^2)

S_{st} = Spacing between stirrups (mm)

Bond slip curve for various level of corrosion derived from above set of equations. Figure-3.6 presents the bond slip behaviour incorporated in the Abaqus. Cohesive element

modelling and cohesive surface modelling are two approaches available to include the bond slip behaviour in Abaqus software. Cohesive element technique generally used to model bond slip behaviour as well as normal behaviour at an interface between two objects. Cohesive element technique is useful to model the thickness behaviour of any interface. Whereas cohesive surface approach is specifically used to model bond slip or tangential behaviour only. Figure-3.6 describes the difference between two techniques. Cohesive surface technique has used to incorporate bond slip behaviour between concrete and steel surfaces in Abaqus software. General contact interaction defined between concrete and steel surface to model the bond behaviour. The general contact interaction allows to model finite sliding between two bond surfaces. Figure-3.7 shows the bond slip curve implemented in the model. The bond slip curve up to maximum bond stress has modified such that it remains as a linear elastic traction separation behaviour before initiation of the damage. However, it has to be ensured that area of curve which represent the energy per unit area remain the same. The increase of bond strength at the initial level of corrosion also can be seen from Figure-3.7.

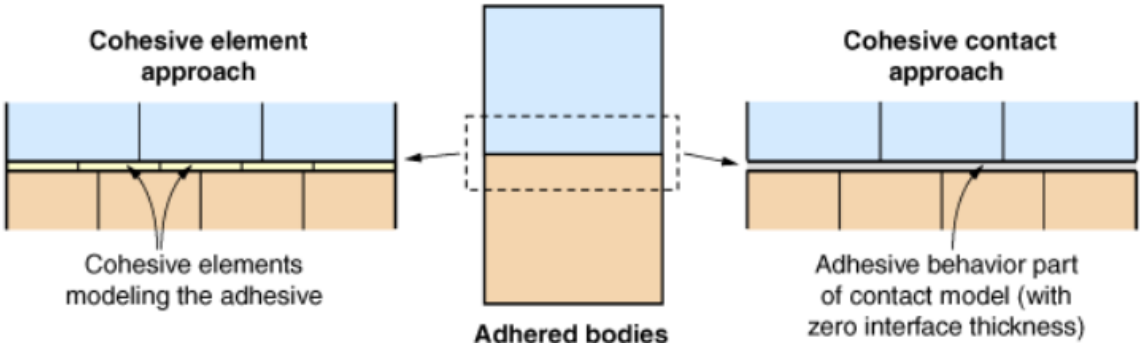

Figure-3.6 Cohesive element and cohesive surface (Abaqus Manual, 2014)

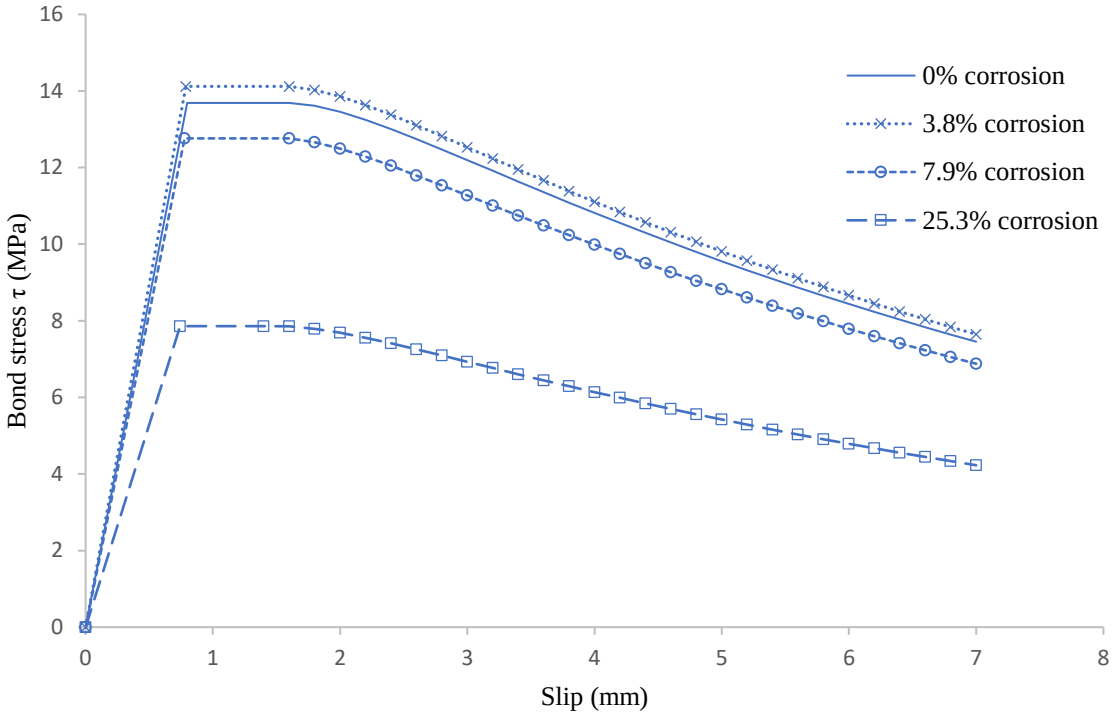

Figure-3.7 Bond-slip behaviour

Cohesive surface properties between an interface of two object defines from the interaction properties in the Abaqus. Three interaction properties normal behaviour, cohesive behaviour and damage had selected from mechanical property option of the interaction property window. In order to prevent any overclosure or detachment between concrete and steel surface, a normal behaviour between two surfaces must define as hard contact. Hard contact option ensures that the concrete surface and steel surface remain in contact with each other throughout the analysis. Normal contact between steel and concrete not only represents the actual situation of rebar and concrete but also ensures the correct implementation of bond slip behaviour in the finite element model. Allow separation after contact option must be tick off to ensure that two surfaces remain in contact through finite element analysis.

Cohesive behaviour defines the linear elastic traction separation behaviour for the interface. The linear elastic behaviour is defined in terms of an elastic matrix as written in Eq. (3.16). It relates the normal and shear stresses to normal and shear separation on the interface.

$$t = \begin{Bmatrix} t_n \\ t_s \\ t_t \end{Bmatrix} = \begin{bmatrix} K_{nn} & K_{ns} & K_{ts} \\ K_{ns} & K_{ss} & K_{st} \\ K_{nt} & K_{st} & K_{tt} \end{bmatrix} \begin{Bmatrix} \delta_n \\ \delta_s \\ \delta_t \end{Bmatrix} = K\delta \tag{3.16}$$

The traction vector t consists of a normal stress and two shear stress components in three directions for the 3D analysis. For 2D analysis it will be one normal stress component and one shear stress component. The δ vector represent the separation (slip) corresponding to stress vector. To model the bond slip behaviour only one longitudinal direction required to define on the interface. Therefore, selecting stiffness coefficients as uncoupled will require $K_{nn}, K_{ss}\ and\ K_{tt}$ values to be define. To define cohesive behaviour in longitudinal tangential direction only K_{tt} value had defined whereas $K_{nn}\ and\ K_{ss}$ values put as zero to restrict cohesive behaviour in the two directions.

Damage modelling requires to define the degradation of bond slip behaviour after the linear elastic bond slip curve at interface. It consists of mainly two variables 1) damage initiation and 2) damage evolution. Damage initiation represents the beginning of the bond strength degradation. To mark the initiation of damage four criteria are available to define the limit of linear elastic bond slip behaviour. Maximum stress criteria, maximum separation criteria, quadratic stress and quadratic damage criteria are applicable to define damage initiation technique. Maximum stress criteria had used in the analysis which marks the beginning of degradation based on stress value. The Eq. (3.17) presents the condition which required to satisfy for initiation of the damage. Input value of maximum bond stress added to define damage initiation.

$$max\left\{\frac{t_n}{t_n^0}, \frac{t_s}{t_s^0}, \frac{t_t}{t_t^0}\right\} = 1 \tag{3.17}$$

Displacement type damage evolution had defined in the FE analysis for the softening curve. As the name suggest damage evolution introduces the softening curve region from the damage initiation point. A tabular format option is selected to achieve the actual softening curve for bond slip behaviour. damage variable (D) determined as shown in Eq. (3.18).

$$D = 1 - \frac{\tau}{\tau_{max}} \tag{3.18}$$

Once the interaction property has been defined in form of cohesive behaviour, the location of interface left to define corresponding to interaction property. The contacts between two objects classified as 1) node to node contact 2) node to surface contact 3) surface to surface contact. Contact formulation technique between two objects depends on the classification of contact. Node to node contact formulation generally used to define bond behaviour between 2D objects in the 2D finite element analysis. Node to surface contact formulation required to define the contact behaviour when the few nodes of one object are in touch with

the surface of another 3D object. Surface to surface contact formulation adopted to define the interaction between two surfaces of the 3D objects. Bond between rebar surface and concrete surface classified as surface to surface contact, since the 3D finite element analysis had performed. Surface to surface interaction implemented with the general contact frame work in the ABAQUS software. In general contact option assign a dummy interaction property consist of normal behaviour as hard contact at the global property assignment. Assign the cohesive interaction property in the individual property assignment option for the corresponding rebar and concrete surface. In this technique it is also feasible to assign a specific bond slip behaviour at each rebar concrete interface based on level of corrosion.

3.4.2 Concrete spalling and cover cracking

Concrete spalling is the effect that has not been included in the finite element model of corroded RC beam in an identical way compared to actual concrete spalling. Thus, not considering the spalling effect in the finite element model had resulted into higher values of load deflection curve. Empirical models considered for the concrete spalling available in the literature always have limited applicability. Therefore, an extensive technique is presented to include the spalling stresses. The spalling stresses in the finite element model of RC beam are identical to actual situation of corroded RC beam.

Analytical model proposed by (El Maaddawy and Soudki, 2007) has used to determine the spalling pressure related to various level of corrosion. The volume increase of the reinforcement due to corrosion is assumed to be twice of the same amount of the reinforcement steel (El Maaddawy and Soudki, 2007). The model relates the spalling pressure to the level of corrosion in a rebar as shown in Eq. (3.19).

$$P_{cor} = \frac{m_1 E_{ef} D}{90.9(1+\nu+\psi)(D+2\delta_0)} - \frac{2\delta_0 E_{ef}}{(1+\nu+\psi)(D+2\delta_0)} \quad (3.19)$$

Corrosion percentage $m_1 = 100\left(\frac{M_{loss}}{M_{st}}\right)$

$\psi = \frac{(D+2\delta_0)^2}{2C[C+(D+2\delta_0)]}$

$E_{ef} = \frac{E}{1+\theta}$

M_{loss} = Mass loss of steel per unit length

M_{st} = Original mass of steel

D = Diameter of steel bar (mm)

C = Min. clear cover thickness (mm)

δ_0 = Thickness of porous zone (mm)

E_{ef} = Effective elastic modulus (MPa)

E = Elastic modulus of concrete

θ = Creep coefficient

ν = Poisson's ratio

The diameter of bar (D), min. clear cover (C), elastic modulus of concrete (E) and corrosion percentage (m_1) consider as per given experiment data for FE analysis. The thickness of porous zone (δ_0) assumed as 0.001 mm, since consideration of porous layer increases the accuracy of the model. The creep coefficient (θ) and Poisson's ratio (ν) assume as 2.35 and 0.2 respectively for concrete.

The volume-increase due to corrosion products at the reinforcement acts as an outward pressure on the concrete. Whereas the reinforcement experience compressive stress due to spalling pressure. The outward normal pressure had applied on the concrete surface, situated at the reinforcement level. The FE model has flexibility to include the different spalling pressure for each reinforcement bar with different level of corrosion. Therefore, finite element model of a corroded RC beam is able to predict more reliable results than others. Experimental RC beams were corroded at various level of corrosion in a laboratory using the accelerated corrosion technique and then tested in a loading frame for the load deflection response. To simulate the same condition in the finite element analysis spalling stresses due to rebar corrosion should be apply from the initial load step to last load step of finite element analysis. Any corroded RC beam consist of a constant spalling stress throughout the test at corresponding level of corrosion. In the Abaqus software the same condition had achieved for spalling stress using the amplitude option. Tabular type amplitude had defined such that the magnitude of applied spalling pressure remains same through FE analysis. Spalling stress has applied at concrete surface using the pressure option available in loads for the finite element model.

3.4.3 Area reduction of the corroded rebar

Corrosion in a reinforcement bar reduces the steel material of the reinforcement. Considering the uniform corrosion along the length of the bar, rebar corrosion reduces the cross-sectional area of the rebar. Reduction in the cross-sectional area of a rebar directly contributes to the degradation of an RC beam. Therefore, it would be necessary to include the effect in the finite element model of a corroded RC beam. A direct reduction in the cross-sectional area of the reinforcement bar would not be possible in the FE model. As the reduction in the cross-sectional area reduces the area of bond surface between steel and concrete and area of spalling stress. Thus, a direct reduction in the cross section area of the reinforcement leads to wrong solution of the finite element analysis for corroded RC beam. Lee *et al.*, (1999) had proposed an empirical technique of reducing the strength of the rebar instead of reducing the cross-sectional area of the rebar. The ultimate strength, elastic modulus, yield strength of the reinforcement bar reduced with increase of corrosion. The formulation which relates the ultimate strength, elastic modulus, yield strength to percentage rebar corrosion are describe as per set of equation presented in Table-3.1.

Table-3.1 Strength of a rebar with percentage corrosion (δw)(Lee *et al.*, 1999)

Type of corrosion	Yield strength (f_{cy})	Ultimate strength (f_{cu})	Modulus of Elasticity (E_{cs})
Uniform corrosion	$\left(1-1.24\left(\frac{\delta w}{100}\right)\right)\times f_y$	$\left(1-1.24\left(\frac{\delta w}{100}\right)\right)\times f_u$	$\left(1-1.24\left(\frac{\delta w}{100}\right)\right)\times E_{ss}$
Pitting corrosion	$\left(1-1.98\left(\frac{\delta w}{100}\right)\right)\times f_y$	$\left(1-1.98\left(\frac{\delta w}{100}\right)\right)\times f_u$	$\left(1-1.24\left(\frac{\delta w}{100}\right)\right)\times E_{ss}$

Although Lee *et al.*, (1999) had proposed the formulation for yield strength and elastic modulus of rebar the reduction in the ultimate strength assumed to decrease at the same rate as yield strength of the rebar. The ultimate strength depends upon the yield strength value in the Lee *et al.*, (1999). Hence the assumption to reduce ultimate strength with corrosion at the same rate as yield strength is valid. This assumption allows to include the actual values of ultimate strength in the finite element model which reported in the literature.

3.5 LOADING AND BOUNDARY CONDITIONS

Application of loading and boundary conditions are very important in any finite element model. They must represent the actual loading condition as well as actual support conditions of an RC beam in the finite element model. Experimental work of corroded RC beams of Rodriguez, *et al.*, (1997) and Lee *et al.*, (1999) consist of four point bending test of all the corroded beam. In order to represent the same boundary conditions in the finite element model rigid plate was created. The rigid plate is able to represent the support conditions of an RC beam for numerical analysis. A discrete rigid shell part had been selected to for the support and loading plates. Since the support plates are completely rigid, Abaqus software require only one node point to determine and calculate the displacement, loads etc. A reference point is required to mark at centre of the support. The reference point marked at the centre of the plate using the partition planes. Dimensions of the plate set as per width of the beam considering the supports placed on the whole width of the RC beam. To assemble all the parts of an RC beam i.e. reinforcement, concrete, stirrups and support plates select the parts in the assemble option. Place the rigid plate at support location and loading points in the assembly option. Figure-3.8 shows the model of an RC beam which is used for finite element analysis.

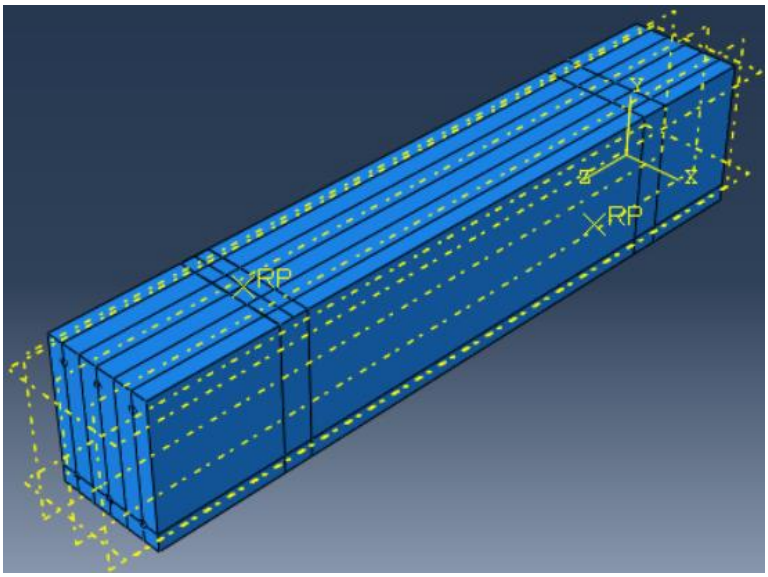

Figure-3.8 Finite element model of an RC beam

The reinforcement of an RC beam arranged in the concrete part using translate, pattern and rotate command in the Abaqus. The uncorroded reinforcement along with stirrups in the concrete part assigned as the embedded region which define the perfect bond between

concrete and steel. The support plates connected with concrete part as a tie constraint to ensure there will not be a slip between support plate and concrete.

Boundary conditions of a finite element model had defined in the initial step so that Abaqus software enable to check the initial stability of the model. The boundary conditions defined at the node of support plates and RC beam. The degree of freedom for the respective boundary condition at each node does not consider in the further iteration analysis. mainly three boundary conditions had applied for an RC beam. The first one is at a support plate which is defined as a hinge support. The second boundary condition is at the middle plane of the RC beam. It defines as the displacement in the two-lateral direction of an RC beam was restrained. The RC beams considered for the finite element analysis are symmetrical along the length. Thus, the finite element model of an RC beam modelled up to half length of the beam with the boundary condition of symmetricity along the length of the beam at middle plane as shown in Figure-3.9. The boundary condition of symmetricity at continuation end of the beam consist of restraining the displacement along the length direction and the rotation in other two lateral direction.

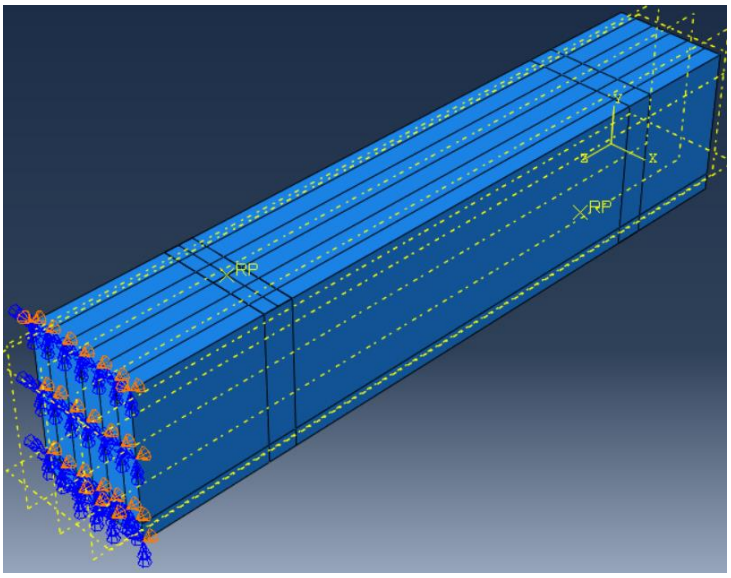

Figure-3.9 Boundary condition at the symmetric plane

Finite element analysis either said to be a load control or displacement control analysis based on the application of loading condition on the finite element model. A displacement control finite element analysis has performed here to achieve the load-deflection curve at ultimate deflection of the RC beam. Since it is certain that the ultimate deflection of an RC beam decreases with increase of corrosion level. A maximum deflection obtained from the control RC beam had applied on all the finite element models of corroded RC beam to

obtain the failure point of a corroded RC beam. Acceleration due to gravity had defined to include the self weight of an RC beam in the finite element model.

3.6 MESH GENERATION OF THE FINITE ELEMENT MODEL

It is assumed that the finite element model made up of homogeneous and isotropic material. Hence, it can be represented in a continuous medium. The continuum medium used to discretize into the different types of elements based on 1D, 2D or 3D finite element model. 1D ,2D and 3D type of finite element model selected to perform numerical analysis based on various factors like importance of analysis, requirement of accuracy and information assumptions etc. A 3D finite element model was prepared to perform the comprehensive finite element analysis of a corroded RC beam. Therefore, model must be discretized into 3D shape of element available in the ABAQUS software. Mainly three types of elements 1) hexahedron 2) wedge and 3) tetrahedron are available to discretize the 3D geometry in the ABAQUS as shown in Figure-3.10.

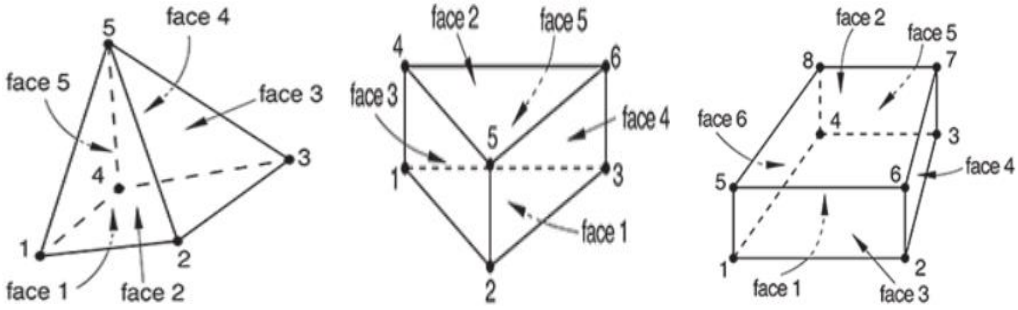

(a) **(b)** **(c)**

Figure-3.10 Available type of elements (a) tetrahedron element (b) wedge element (c) hexahedron element (Abaqus Manual,2014)

Selection of type of element is based on the finite element analysis and geometrical shape of model. hexahedron element is preferred to select in which bending stresses govern the behaviour of a finite element model. Whereas tetrahedron element used to select for shear stress dominant finite element analysis. 8 node hexahedron elements have selected for concrete and steel reinforcement of the RC beam. 2 node 1D bar element was selected for the stirrups bar of the RC beam.

In order to perform accurate and divergence free finite element analysis it is very important to have a uniform type of element to represent a continuous medium. Moreover, the bond behaviour can be implemented using the linear interface element in the Abaqus software.

Therefore, the two body must be of linear element i.e. 8 node hexahedron, 5 node tetrahedron between which the bond model is required to incorporate. Hence, linear elements had chosen instead of quadratic elements for the concrete and reinforcement material of an RC beam model. Size of hexahedron element selected as 30 for the RC beam model. Figure-3.11 shows the meshing of the RC beam model.

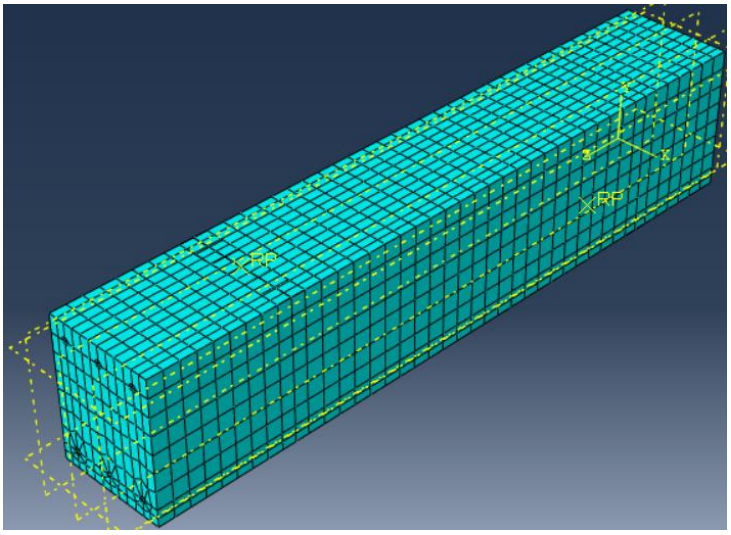

Figure-3.11 Meshing of the RC beam model

3.7 METHOD OF ANALYSIS

Various types of methods are available in the Abaqus to perform finite element analysis based on their objectives. The method of analysis defined in each step of the model. A nonlinear static analysis is required to perform for the RC beam subjected to static loading. Hence the static general type of analysis was selected at the time of defining step-1 in the Abaqus. Nonlinear static analysis neglects the effect of inertial force as well as effect of time period. Although time period had defined as 1unit value to relate the rate of loading in the amplitude option. Load step increment selected as automatic to avoid any convergence issue due to size of increment. The Newton Raphson iteration method used for the nonlinear static analysis in the Abaqus.

CHAPTER-4

RESULTS AND DISCUSSION

4.1 OVERVIEW

The present chapter discusses about the results and comparisons of finite element analysis to the experimental study of Rodriguez *et al.,* (1997) and Lee *et al.,* (1999). Effect of the corrosion on the flexural behaviour of an RC beam has observed through finite element analysis. Spalling stress variation data extracted from the performed finite element analysis. Demonstrate an attempt to establish relation between spalling stress variation to global load deflection behaviour of the corroded RC beam in order to develop a better understanding of corrosion mechanism. Verified finite element model extended to finite element analysis of multiple level of corrosion in the RC beam in order to obtain the effect of corrosion at a sustainable loading on the RC beam. Optimum maintenance point for the corroded RC beam has defined based on the design load and serviceability criteria of the beam as per IS:456-2000.

4.2 DESCRIPTION OF THE FE MODEL OF RC BEAMS

The present study involves numerical investigation of two different experimental works carried out by Rodriguez *et al.,* (1997) and Lee *et al.,* (1999). Both the studies considered RC beams and included the effect of corrosion through accelerated corrosion technique. The detailed description and the numerical study for each of the beams is discussed one by one. Two different set of experimental work has selected to compare the results of finite element analysis with the respective experimental results. The comparison of results confirms the larger applicability and acceptance of the finite element technique to include corrosion effects. RC beam specimen of Lee *et al.,* (1999) consist of 6 mmϕ stirrups bar at 50 mm c/c and corrosion in the tension reinforcement of the RC beam only. Hence confinement effect of concrete is involved in the experimental specimen. Whereas RC beam specimen of Rodriguez *et al.,* (1997) consist of 6 mmϕ stirrups bar at 170 mm c/c and corrosion in all the reinforcement bar of the RC beam. Hence there will not be any confining effect of concrete. The actual bond strength degradation is less for confined concrete whereas it is high in the other set of RC beam specimen. Therefore to check the

applicability of the bond model and finite element model under various circumstances, two different set of experimental work has been selected for validation.

4.2.1 Validation of numerical analysis with Lee *et al.,* (1999)

The considered RC beam (Lee *et al.,* 1999) is of cross section 200 mm x 250mm with overall length of 2 m as shown in Figure- 4.1a and 4.1b. The reinforcement detailing, geometry, and the detailed cross-sectional dimensions in the beam are also shown in Figure 4.1a and 4.1b. A corrosion free RC beam specimen termed as control specimen (BS) tested along with corroded RC beam specimen BCD1 (3.8%), BCD2 (7.9%) and BCD3 (25.3%) at respective level of corrosion on the tension reinforcement. Level of corrosion on rebar was measured by weight loss of the rebar. Four-point bending test had carried out on each RC beam to plot load vs deflection curve.

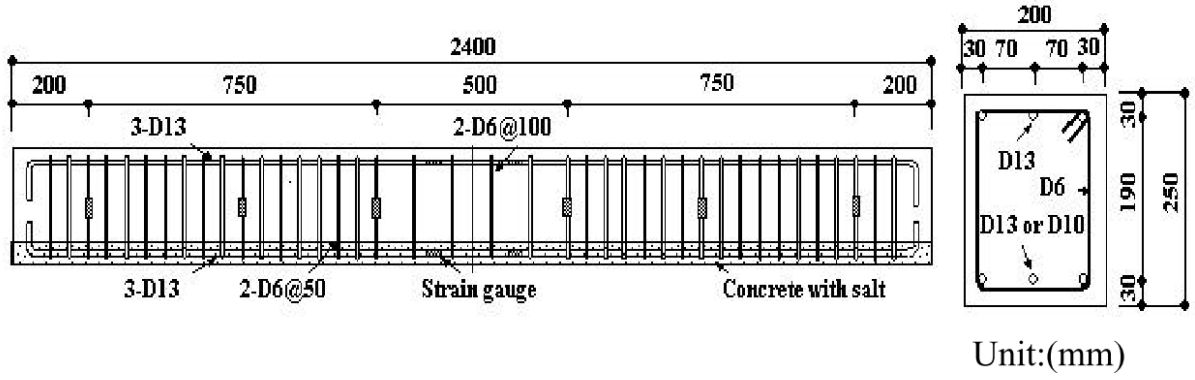

(a) **(b)**

Figure 4.1 Details of the RC beam considered (Lee *et al.,* 1999) (a) Elevation (b) Cross section

Table-4.1 Material properties of the RC beam (a) Concrete (b) Steel (Lee *et al.,* 1999)

W/C (%)	s/a (%)	Slump(cm)	Unit Weight(kg/m^3)				Fc (MPa)	E_c (MPa)	N
			W	C	S	G			
65	45	18	185	285	776	1007	39.2	29419	0.19

(a)

Rebar (mm)	Yield strength (N/mm^2)	Tensile strength (N/mm^2)	Elastic Modulus (GPa)
13	343	477	182
6	226	415	192

(b)

The stress strain curve for concrete in compression and tension has generated based on the reported properties of concrete and the Equations (3.2), (3.3) and (3.7). Figure-4.2a and 4.2b shows the stress strain curve defined for concrete in compression and tension in the finite element model. The stress strain curve of reinforcement defined as shown in Figure-4.3a and 4.3b for the control RC beam. The stress strain relationship for reinforcement is modified based on the Equation from Table-3.1 of uniform corrosion type. Specific values of yield strength and ultimate strength is considered for each type of reinforcement as reported by Lee *et al.*, (1999). Ultimate strain value for reinforcement is adjusted such that maximum deflection for control RC beam obtained from the finite element analysis is same as experimental value. It is remained the same for the rest of finite element analysis of corroded RC beams.

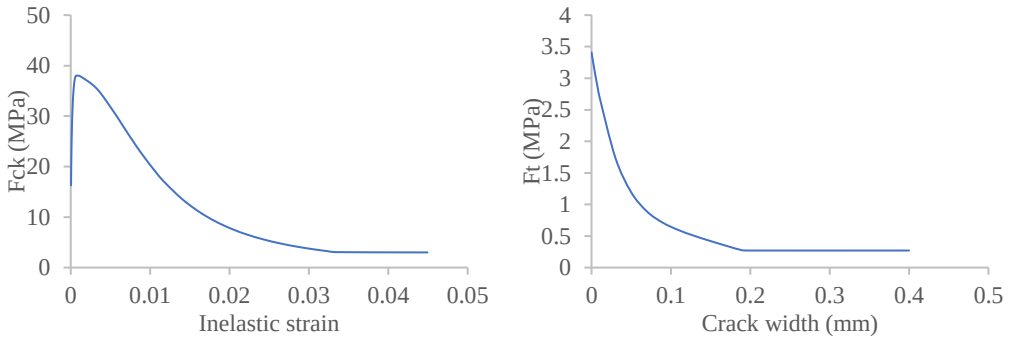

(a) **(b)**

Figure-4.2 Concrete properties (a) in compression (b) in tension

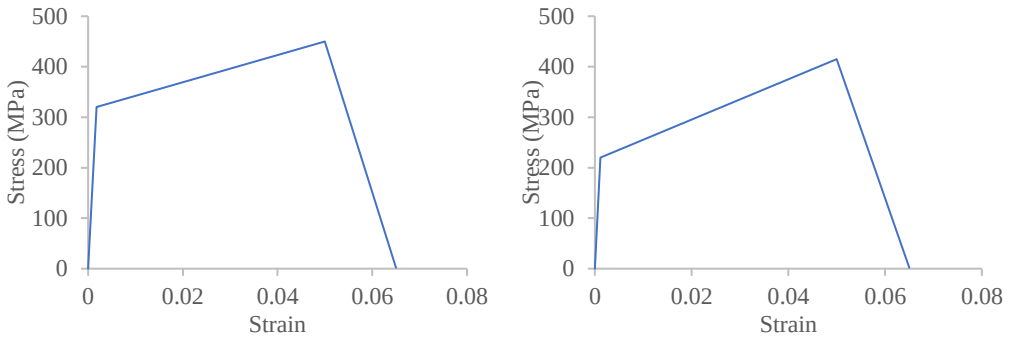

(a) **(b)**

Figure-4.3 Stress-strain curve for reinforcement (a) Longitudinal rebar (b) Stirrups

Using these properties for steel and concrete, a displacement control finite element analysis was carried out in the Abaqus software. Average increment step size of the displacement control analysis is 0.12 mm. A deflection value 90 mm is applied in the finite element model such that RC beam fails before reaching the particular deflection to identify the failure point of a beam.

Figure 4.4 shows the load versus displacement plot of the bending test performed on the RC control beam as obtained from experimental investigation and numerical analysis. The results of the present study correlates well with those obtained in the experimental study (Lee at al 1999).

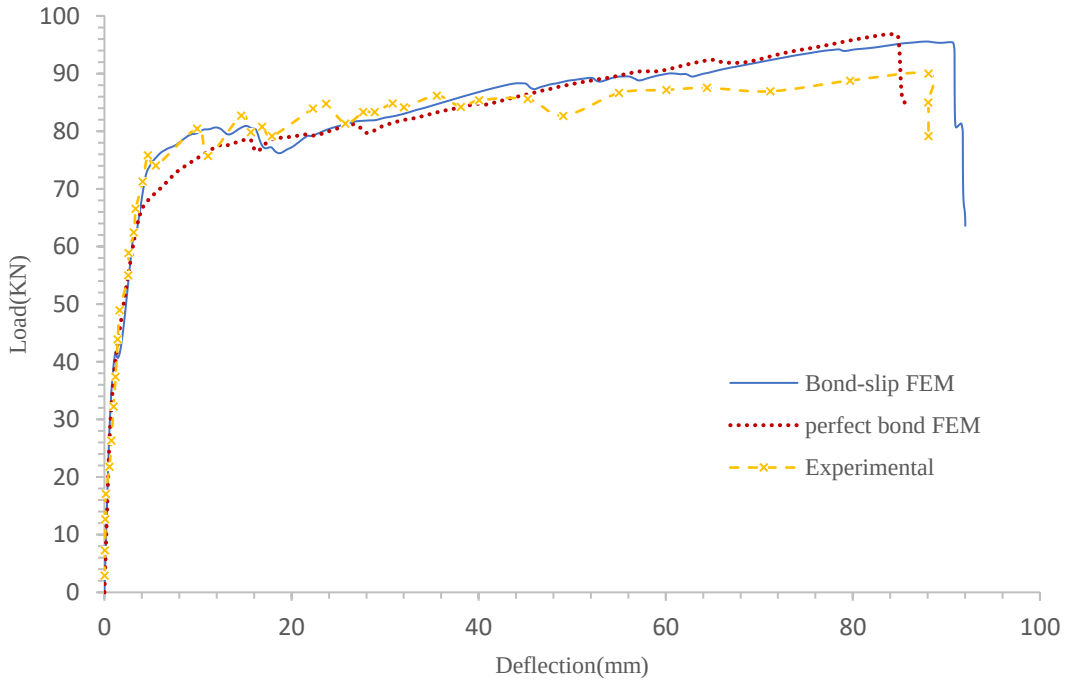

Figure-4.4 Load vs Deflection curve for control RC beam (BS)

Various researchers have proposed their empirical bond model based on their experimental investigation(Cabrera, 1996; Chung *et al.*, 2004; Bhargava *et al.*, 2007; Jiang, *et al.*, 2018). The bond model of Jiang *et al.*, (2018) is implemented for the FE analysis of the corroded RC beam. Hence as a verification of the bond model, it must represent the perfect bond at 0% corrosion between steel and concrete. A cohesive surface defines the bond-slip behaviour between concrete and steel surfaces in normal and tangential directions on the surface. The Bond model is verified for a corrosion level of 0% with that a perfect bond condition in terms of the load vs deflection plots as shown in Figure-4.4. A perfect bond between reinforcement and concrete defined through embedded region constraint in the ABAQUS. The comparison of load versus displacement curves of the two-modelling approach shows a good tally between them implying that the adopted bond- slip model works well for the considered numerical model.

Once the bond-slip model validated with 0% corrosion, bond-slip behaviour for 3.8%, 7.9% and 25.3% corrosion level had incorporated in the finite element model. To incorporate the corrosion in the finite element model one has to include 1) reduction in strength of the rebar 2) bond-slip behaviour and 3) spalling stresses included in the FE model based on the level of corrosion. Corrosion effects applied to the bottom bars of the RC beam and rest of the reinforcement bars modelled as a perfect bond condition with concrete. Numerical analysis of the RC beam at the respective level of corrosion performed for each finite element model. The load-deflection curves of the corroded RC beams are as shown in Figure-4.5.

Table-4.2 presents the comparison between experimental and FEM results for cracking load, yield load and a maximum load of the corroded RC beam. % deviation for yield load and maximum load compared to experimental results are well below 5% and 10% respectively. While for cracking load at 25.3% corrosion level numerical analysis result contradicts with experiment results. Cracking load of corroded RC beam is expected to decrease with the increase of corrosion level.

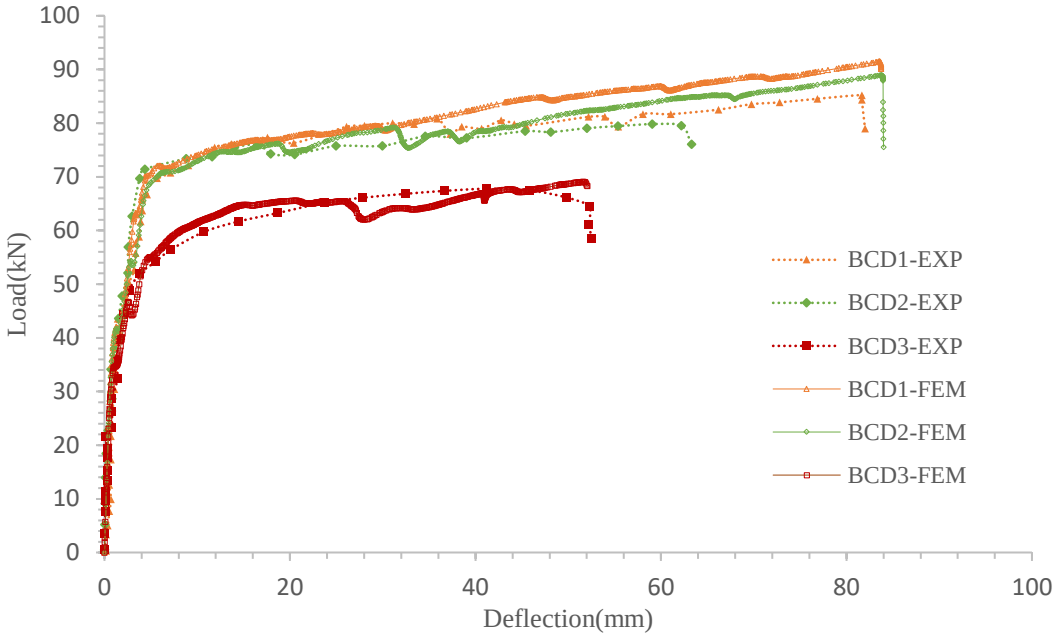

Figure-4.5 Comparison of Load-Deflection curve for corroded RC beam

It has been observed that corrosion effect on % reduction of cracking load is less compared to the yield load and the maximum load of the RC beam. While % reduction in the yield load and the maximum load of the RC beam remain similar to each other with the increase of corrosion.

Table-4.2 Comparison of experimental and FEM results at (a) Cracking load (b) yield load and (c) Maximum load

RC beam type	ΔW (%)	Cracking load (KN)		% Reduction
		Experiment	FEM	
BS	0	22.6	23.34(3.3%)	0
BCD1	3.8	21.6	23.39(8.2%)	0
BCD2	7.9	20.6	23.5(14.07%)	0
BCD3	25.3	24.5	21.6	7.50%

(a)

RC beam type	ΔW (%)	Yield load (KN)		% Reduction
		Experiment	FEM	
BS	0	75.5	74.40(1.5%)	0
BCD1	3.8	71.1	71.40(0.4%)	4.03%
BCD2	7.9	69.6	69.27(1.5%)	6.90%
BCD3	25.3	51.5	53.4(1.9%)	28.23%

(b)

RC beam type	ΔW (%)	Maximum load (KN)		% Reduction
		Experiment	FEM	
BS	0	88.9	94.58(6.4%)	0
BCD1	3.8	85.4	91.45(7.08%)	3.3%
BCD2	7.9	78.8	88.6(12.43%)	6.32%
BCD3	25.3	67.3	68.26(1.4%)	27.83%

(c)

It has been also observed that deflection at the yield load and the maximum load of the RC beam decreases with the increase of corrosion. Ultimate deflection point of an RC beam obtained as 90.7 mm, 83.66 mm, 83.91 mm and 52 mm for control RC beam, 3.8%, 7.9% and 25.3% corroded RC beam respectively. The evolution of deflection value at yield load and at failure of RC beams mark the increase in the brittle behaviour with increase of corrosion level. Ultimate deflection point for 3.8% and 25.3% corroded RC beam shows good match between experimental and numerical results. The ultimate strain of steel bar governs the ultimate deflection of the corroded RC beam. The strain in the steel bar reaches quickly at the ultimate point in case of corroded bar compared to healthy rebar. Few researchers (Castel *et al.*, 2000; Coronelli and Gambarova, 2004; Biondini and Vergani, 2014) have proposed empirical relation between loss of ultimate strain in steel bar with the level of corrosion. However, these empirical relations limited to the particular set of experimental results. Since there is no data available on the ultimate strain value of corroded rebars. The ultimate strain value had adjusted based on the ultimate deflection of the control RC beam and then it remains the same for the rest of the corroded RC beam analysis.

The relative decrease in load carrying capacity and energy of corroded RC beam is shown in Figure4.6a and 4.6b. The trend of decreasing load carrying capacity (maximum load) with increase of corrosion level is well comply with results presented in the literature(Dekoster *et al.*, 2003; Yu *et al.*, 2015). Total energy parameter is calculated for each RC beam by the integration of the load-deflection curve for the respective RC beams. Since the ultimate capacity and the ultimate deflection of RC beam both influence the total energy of an RC beam, relative energy curve may differ from the maximum load curve of Figure-4.6a. The relative energy (E/E_{max}) is the ratio of the total energy of corroded RC beam to total energy of control RC beam.

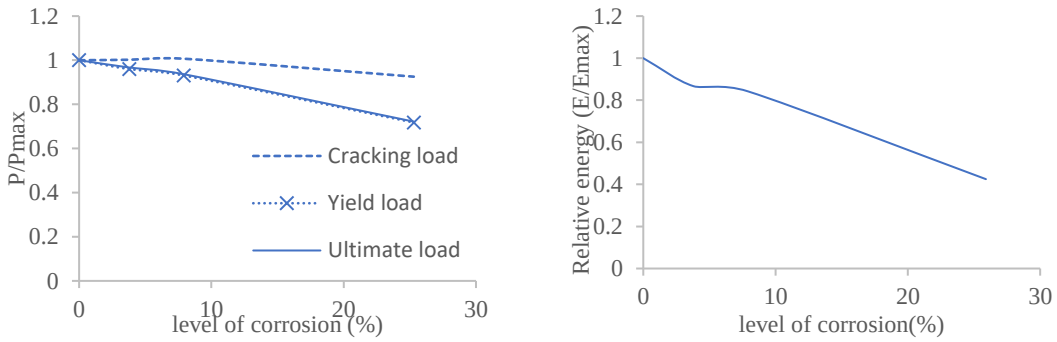

(a) **(b)**

Figure-4.6 (a) relative ultimate capacity vs level of corrosion (%) (b) relative energy(E/E_{max}) vs level of corrosion (%)

Flexural cracks region of the RC beam used to identify with max. principal strain parameter in the FE model. Figure-4.7a and 4.7b presents the comparison of max. principal strain region between control RC beam and 25.3% corroded RC beam. It is clear from Figure-4.7 that flexural crack region reduces with the increase of corrosion level in the RC beam (Lee *et al.*, 1999). Also, as the level of corrosion increases, the failure mechanism of RC beam leans from flexural failure to shear failure(Lee *et al.*, 1999).

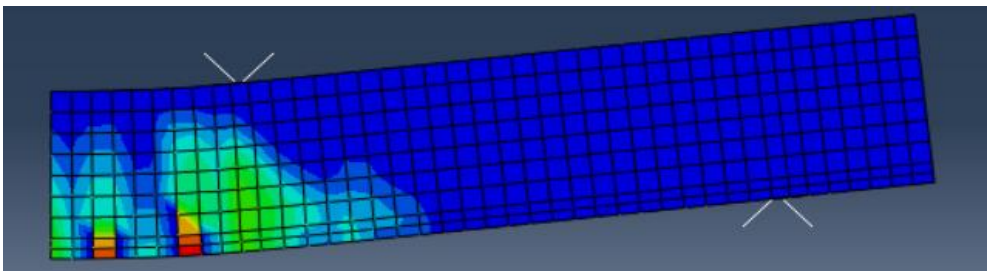

(a)

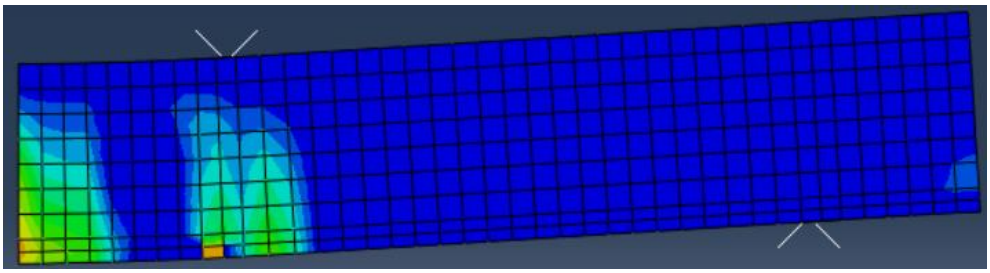

(b)

Figure-4.7 Distribution of maximum principal strain (a) RC control beam (b) Corroded RC beam (25.3%)

FE model shows cover cracking/spalling effect on the cross-section of the RC beam. Figure-4.9 presents the Von Mises stress distribution on the cross section for all the four specimens. 1st increment step of the respective finite element analysis selected to display the spalling effect at section A-A' shown in Figure-4.8. The cross-section of RC beam at section A-A' is selected to present the spalling stresses in the beams. It is the cross-section with the least bending stresses due to loading. Difference between Figure-4.8(a) control RC beam and Figure-4.7(b) 25.3% corroded RC beam clearly explains the importance of including actual spalling stresses in the numerical analysis. Comparison between Figure-4.8b, 4.8c and 4.8d also shows that distance between two rebars also plays an important role in cover cracking of concrete. Thus, cover cracking of concrete mainly governs by the level of corrosion, the strength of concrete, clear cover and distance between two corroded rebars.

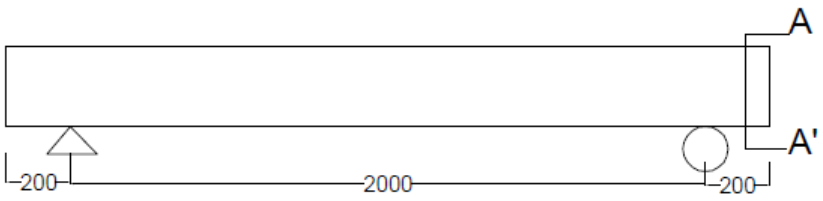

Figure-4.8 Section A-A' on the RC beam

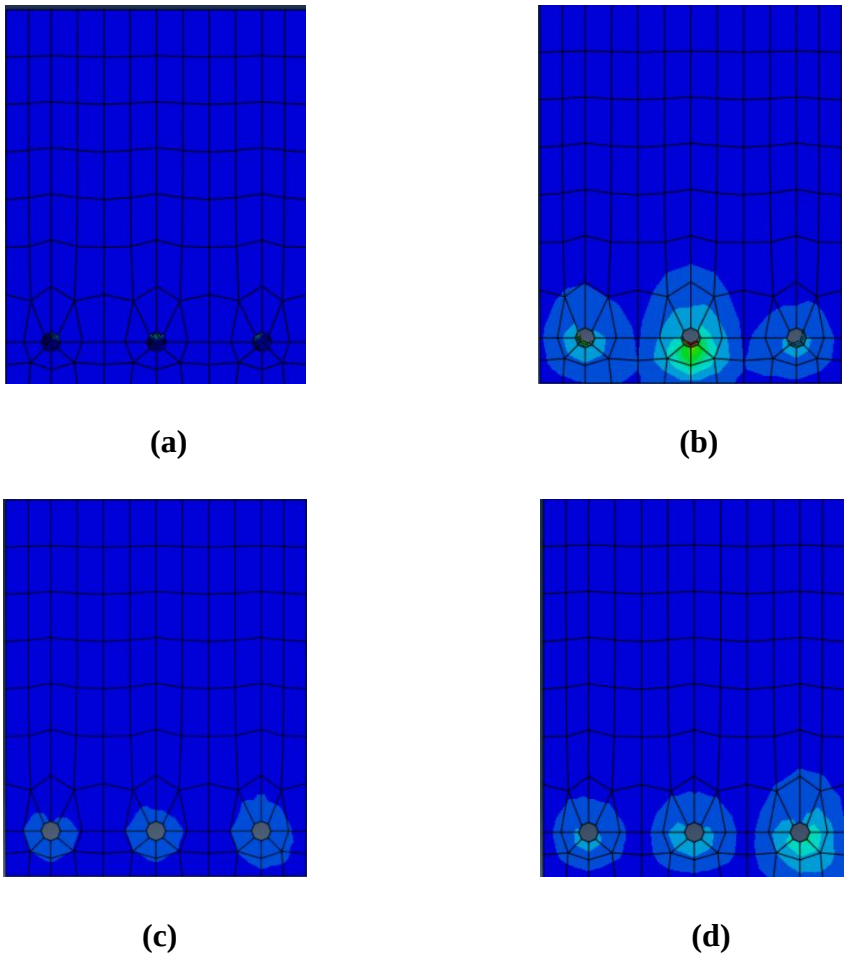

(a) **(b)**

(c) **(d)**

Figure-4.9 Distribution of Von mises stress at section A-A' for (a) BS (b) BCD1 (c) BCD2 (d) BCD3

In order to check the effect spalling stress, a corroded RC beam of 25.3 % corrosion has analysed for no spalling stress with the same bond properties and strength of rebars. Only bond strength degradation and reduction of strength of the steel bar is considered in case of corroded beam without spalling. Figure-4.10 shows the load vs deflection curve obtained from finite element analysis with and without inclusion of spalling stress in the finite element model of a corroded RC beam. The effect of spalling stress due to rebar corrosion has observed mainly in the plastic region of the 25.3% corroded RC beam. It is observed that the effect of spalling stress due to rebar corrosion is dominant mainly in the plastic region of the corroded RC beam. Even though the ultimate displacement of the RC beam is different in both the cases, but the failure of the corroded RC beam in both cases occurred due to bond failure, as the ultimate stress in the steel bar could not be reached in the finite element analysis of the RC beam.

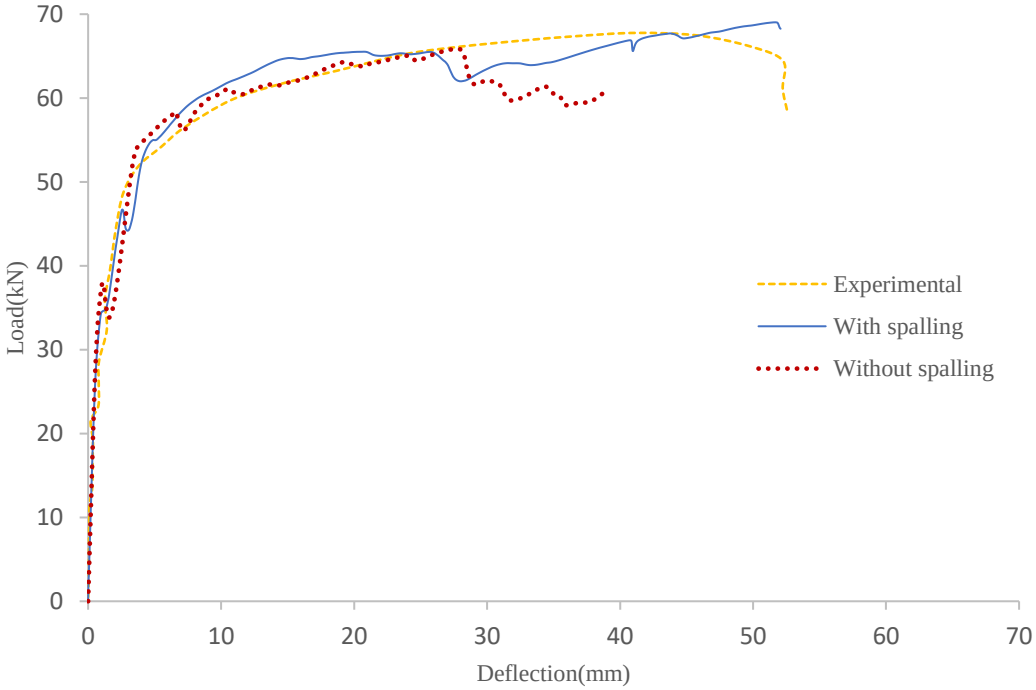

Figure-4.10 load-deflection curve for spalling and without spalling

It is also observed that the spalling pressure acting opposite side of loading on the RC beam contribute to strengthen the global behaviour of the RC beam. The spalling pressure applied along the loading direction of the RC beam is responsible for the cracking of the cover concrete. The Figure-4.11 shows the schematic diagram of steel concrete interface subjected to spalling stresses. The spalling pressure due to rebar corrosion which acting in opposite direction of the loading increases the load deflection value slightly higher than without spalling condition.

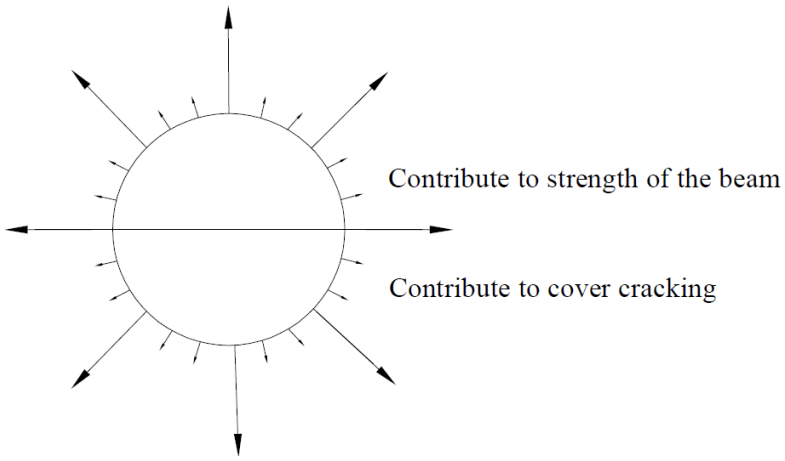

Figure-4.11 Schematic diagram of steel concrete interface subjected to spalling stresses

Although overall load deflection curve modifies due to bond strength degradation and strength of the rebar. A small amount of spalling stresses in the plastic region lead to minimal increase in the strength of the corroded RC beam. Therefore, a minor increase in load carrying capacity resulted into higher ultimate deflection of the RC beam. Hence the spalling stresses due to corrosion also influence the ultimate deflection point of the RC beam. Therefore, the ultimate deflection point of any corroded RC beam is governed by combined mechanism of ultimate strain of steel bar, bond strength and spalling stresses.

4.2.2 Validation of numerical analysis with Rodriguez *et al.,* (1997)

Rodriguez *et al.,* (1997) did experiments on various types of RC beam for various level of corrosion. One set of RC beams has considered for the comparison with FE analysis. This comparison is intended to authenticate the applicability of the FE model over various conditions. Geometric detail of the RC beam has shown as per Figure-4.12. Unlike (Lee *et al.,* 1999)'s beam, all the reinforcement are uniformly corroded at various level of corrosion. RC beams had been corroded up to the desired level of corrosion with Accelerated corrosion technique. Two types of concrete mix prepared 1) control RC beams and 2) corroded RC beam which consists of calcium chloride. Calcium chloride ($CaCl_2$) was added to mixing water in the concrete mix to accelerate the reinforcement corrosion process. Concrete properties of RC beams have shown in Table-4.3. Plasticizer plastiment HP-1 additionally added to both types of the concrete mix in quantity of 1.75 Kg/m^3. Properties of rebar are as shown in Table-4.4.

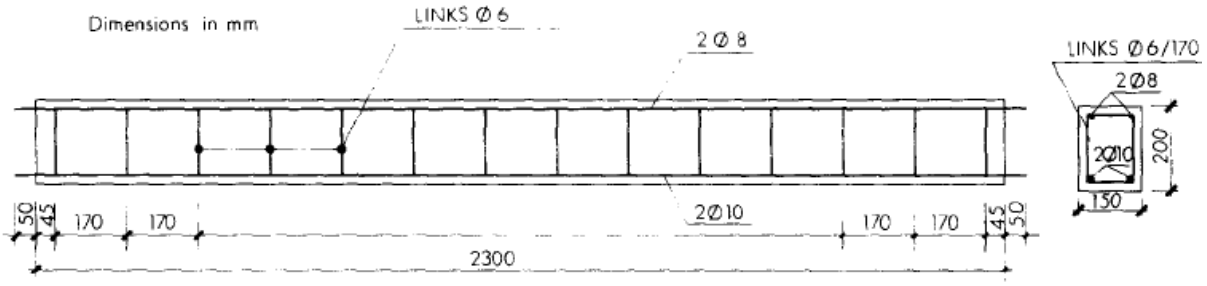

Figure-4.12 Detail of RC beam

Table-4.3 Material properties of considered RC beam (a) concrete (b) Steel (Rodriguez *et al.*, 1997)

Concrete type	W/C	Slump (cm)	Unit Weight(kg/m3)				$CaCl_2$ (Kg/m^3)	Fc (MPa)	N
			W	C	F.A.	C.A.			
1	50	5-8	175	350	860	970	-	50	0.19
2	50	12-18	175	350	860	970	10.5	34	0.19

(a)

Bar dia.	Yield strength (N/mm^2)	Ultimate strength (N/mm^2)	Elastic Modulus (GPa)
6 mm	626	760	200
8 mm	615	670	182
10 mm	570	650	182

(b)

The stress strain curve for concrete in compression and tension generated based on reported properties of concrete. The convenient input parameters had chosen to define the stress strain curve in concrete damaged plasticity model in ABAQUS. Figure-4.13a and 4.13b shows the properties of concrete for concrete type 1 which was used for the control RC beam (H) specimen. Figure-4.14a and 4.14b shows the properties of concrete defined for the corroded RC beams (C1, C2 and C3).

The stress strain curve for reinforcement defined in the ABAQUS as shown in Figure-4.15. The stress strain curve for concrete in compression and tension generated from the Eq.-(3.2), (3.3) and (3.7). Specific values of yield strength and ultimate strength is considered for each type of reinforcement as reported by Rodriguez *et al.*, (1997).The stress strain relationship is modified based on the equation from Table-3.1 of uniform corrosion type.

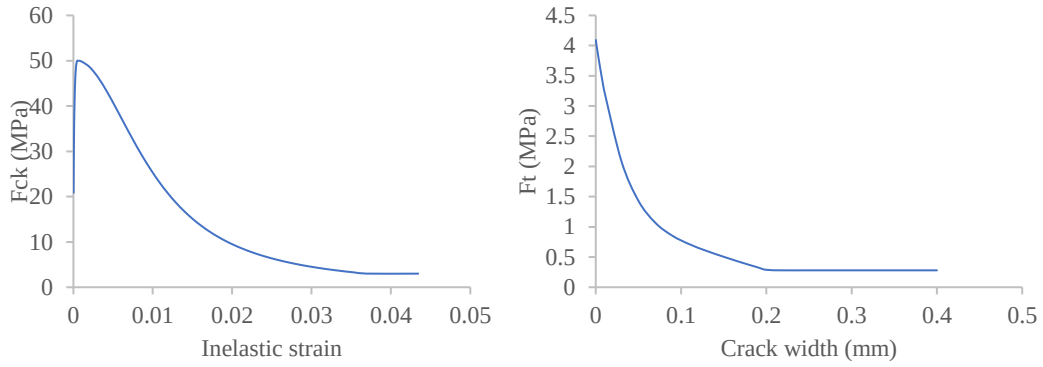

(a) **(b)**

Figure-4.13 Properties of concrete type 1 (a) in compression (b) in tension

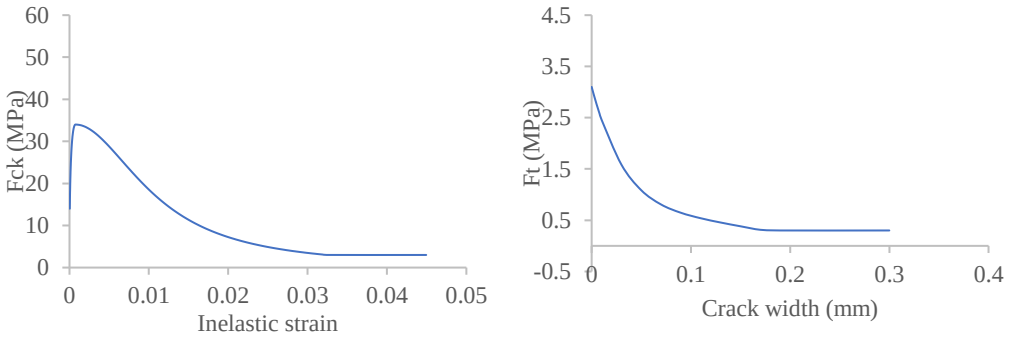

(a) **(b)**

Figure-4.14 Properties of concrete type 2 (a) in compression (b) in tension

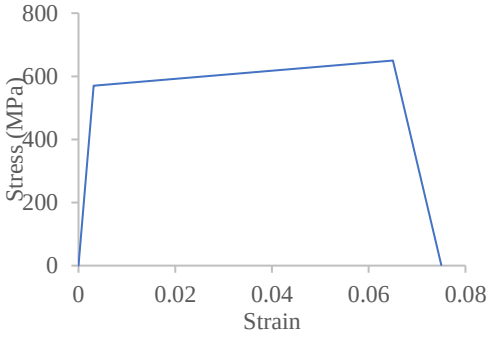

Figure-4.15 Stress strain curve for reinforcement

Three corroded RC beam and a control RC beam results selected out of all experimental specimen for comparison with numerical analysis. Level of corrosion in each RC beam and rebar is presented in Table-4.4. different level of corrosion had incorporated for top bars, bottom bars and stirrups in the experiment. Corrosion effects due to corrosion of longitudinal rebars have included in finite element analysis. Only strength reduction due to corrosion of the rebar has considered for corroded stirrups in finite element analysis. The

volume increase due to corrosion is assumed to be twice of the same amount of rebar steel(El Maaddawy and Soudki, 2007).

Table-4.4 Corrosion level of reinforcement

Beam type	Concrete type	Depth of corrosion (mm)		
		Bottom bars	Top bars	Stirrups
H (11.1)	1	-	-	-
C1 (11.4)	2	0.45(17.2%)	0.52(24.31%)	0.39(24.31%)
C2 (11.5)	2	0.36(13.88%)	0.26(12.58%)	0.37(23.15%)
C3 (11.6)	2	0.70(26.04%)	0.48(22.56%)	0.68(39.16%)

Bond degradation, spalling stresses and strength reduction effect include based on the level of corrosion on each reinforcement in all the corroded RC beams. As an advantage of this finite element analysis, spalling stresses can be included on each rebar based on a specific level of corrosion in the rebar. Figure-4.16 presents the comparison of the load-deflection curve between FE analysis and experimental results for control RC beam (11.1). (Coronelli and Gambarova, 2004) had performed finite element analysis on the same set of experimental RC beam in their study. For the comparison of the accuracy of the finite element analysis, load-deflection curve of (Coronelli and Gambarova, 2004) for the same RC beam has plotted in Figure-4.16. FEM result of the H RC beam is well matched with experimental results of (Rodriguez, *et al.,* 1997). Although the initial elastic region of the experimental result did not agree with finite element analysis outcome, FEM result from cracking load remain close with the experimental outcome.

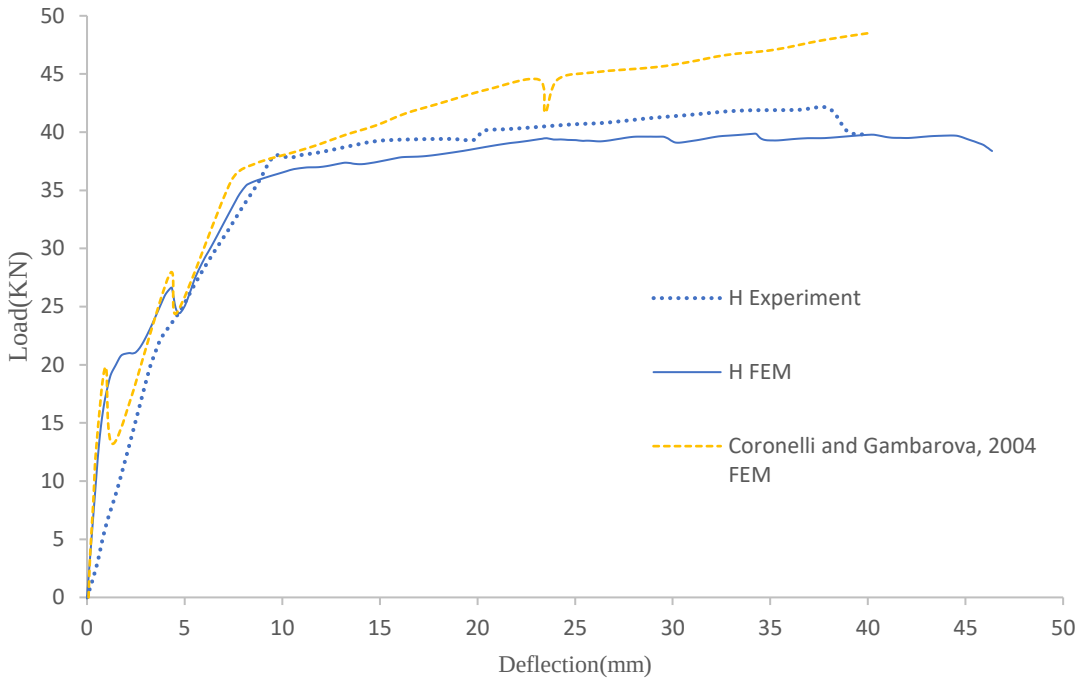

Figure-4.16 Load vs Deflection curve for control RC beam H

Finite element analysis for corroded RC beams C1, C2 and C3 had been performed in ABAQUS. The results are compared with experimental data as well as FE analysis data of (Coronelli and Gambarova, 2004). Figure-4.17a, 4.17b and 4.17c shows the comparison of load-deflection curve for experimental and numerical analysis results. Apart from the initial elastic region, the FE analysis results for corroded RC beams show a good match with experimental results. Comparison between experimental and FEM results at ultimate load point and yield load point for each RC beams presents in Table-4.6. It has been observed that the finite element analysis gives around 18.67% higher load deflection value compared to the experimental values in case of C3 corroded RC beams. Higher values of FE analysis results may be attributed to the spalling effect of corroded stirrups. Stirrups corrosion does affect the concrete spalling(Lin *et al.*, 2017), which is not consider in the present study. Stirrups bars modelled as 1D beam elements in the finite element model. spalling effect and bond degradation effect are not included for stirrups corrosion in the finite element model. Likely reason for higher values of finite element analysis is neglecting the effect of concrete spalling due to stirrups corrosion. Overall methodology to capture the effect of corrosion using the finite element analysis has verified with two different sets of experimental data.

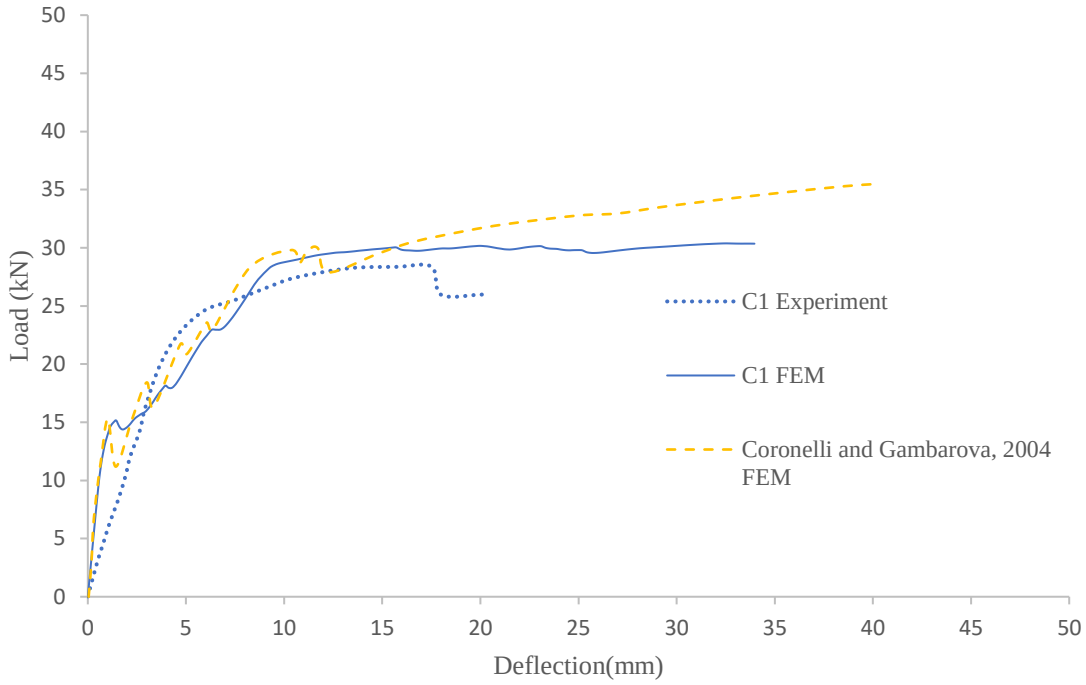

(a) Corroded RC beam C1

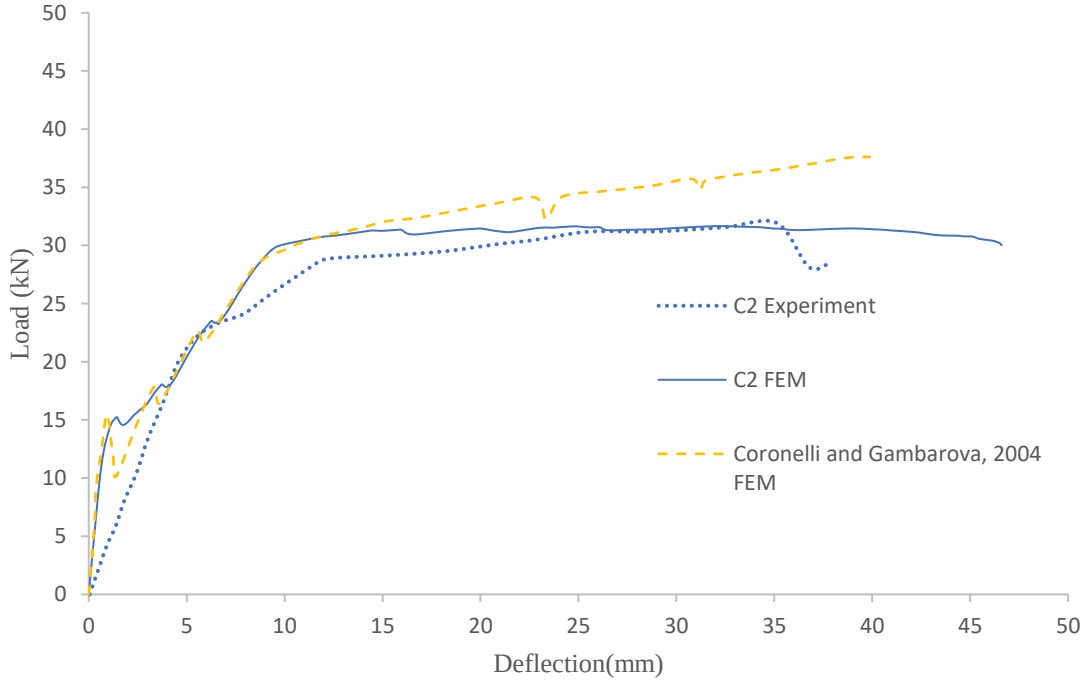

(b) Corroded RC beam C2

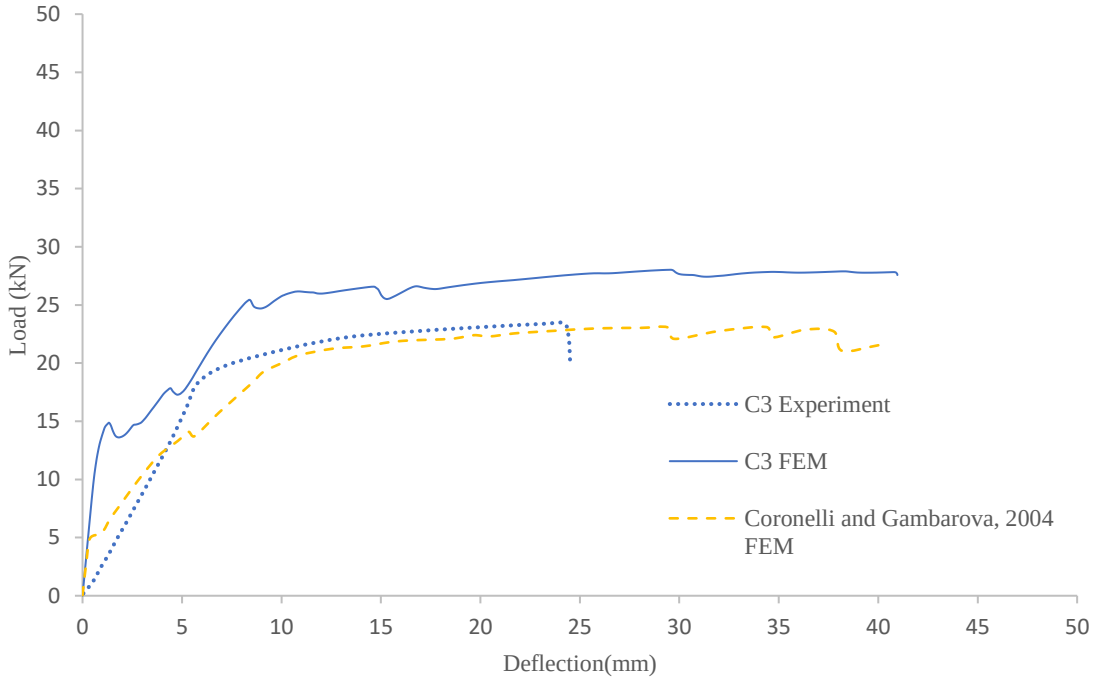

(c) RC beam C3

Figure-4.17 Load vs Deflection curve for corroded RC beam (a) C1 (b) C2 and (c) C3

Table-4.5 Comparison of experimental and FEM results

Beam type	Yield load (KN)		Ultimate load (KN)	
	Experiment	FEM	Experiment	FEM
H	37.88	35.50(6.28%)	42.05	39.55(5.95%)
C1	24.67	28.22(14.38%)	28.38	29.95(5.53%)
C2	28.77	29.57(2.78%)	31.92	31.59(1.03%)
C3	20.29	24.08(18.67%)	23.42	27.5(17.42%)

Maximum principal strain distribution has shown in Figure-4.18 to compare the flexure crack region between control RC beam H and corroded RC beam C3. As the corrosion level in the rebars increases, RC beam tends to fail more due to shear instead of flexure. Fig - 4.14 presents the failure scenario of a healthy RC beam and a corroded RC beam. Flexural cracks region for corroded RC beam has significantly reduced under the effects of corrosion.

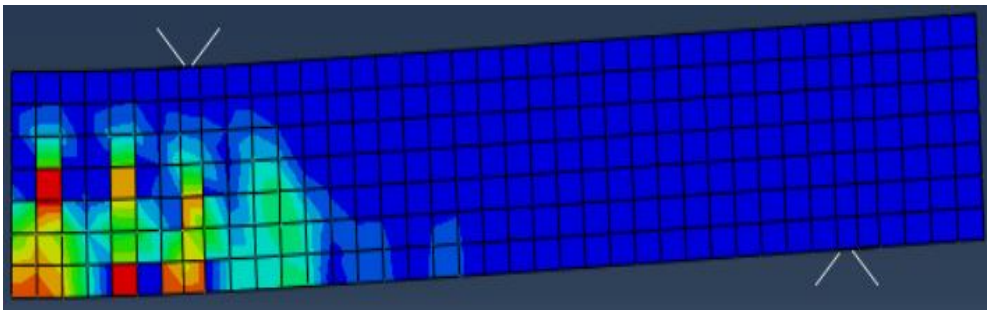

(a)

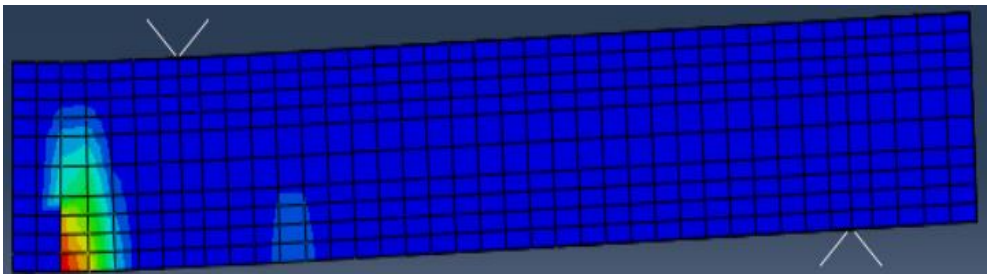

(b)

Figure-4.18 Distribution of maximum principal strain (a) 11.1 RC beam (b) 11.6 RC beam

Concrete spalling stresses of corroded RC beam can be seen through von Mises stress distribution in the cross-section of the RC beam. Figure-4.19 shows the location of the cross-section for presenting the effect of spalling stress. Figure-4.20a and 4.20b present the comparison of stress distribution for healthy RC beam and corroded RC beam at section A-A'

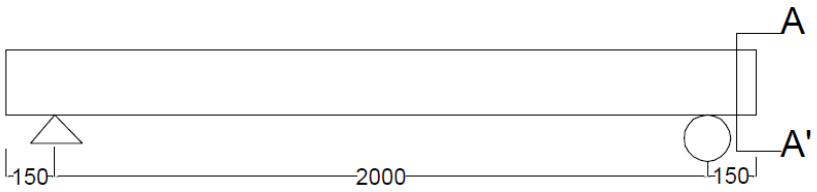

Figure-4.19 Section A-A' on the RC beam

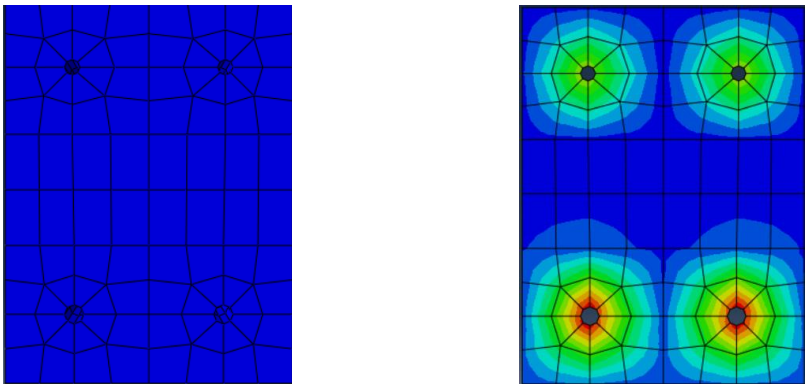

(a) **(b)**

Figure-4.20 Distribution of Von mises stress at section A-A' (a) H beam (b) C3 beam

4.3 SPALLING STRESS VARIATION

The effect of uniform corrosion in rebar on an RC beam has studied with the help finite element analysis. The spalling stresses induced on the concrete due to corrosion of rebar is applied in form of a constant outward pressure on the adjacent concrete surface in the finite element model of the beam. It is observed that the spalling stresses around the corroded bar vary under the influence of bending stresses of the RC beam. To understand it in greater depth, a detailed study has been conducted to find out the influence of bending stresses on a corroded RC beam Rodriguez *et al.*, (1997). Three different sections, A-A′, B-B′ and C-C′ (Figure 4.21a) are selected along the length of the RC beam from support to mid-span to represent the variation of spalling stresses. Sections are selected such as each section are subjected to different level of bending stresses. A typical cross section of the considered beam is shown in Figure 4.21b. Figure 4.21c shows the different locations (circular angles) considered for the spalling stresses and location of the interface on the cross section of an RC beam.

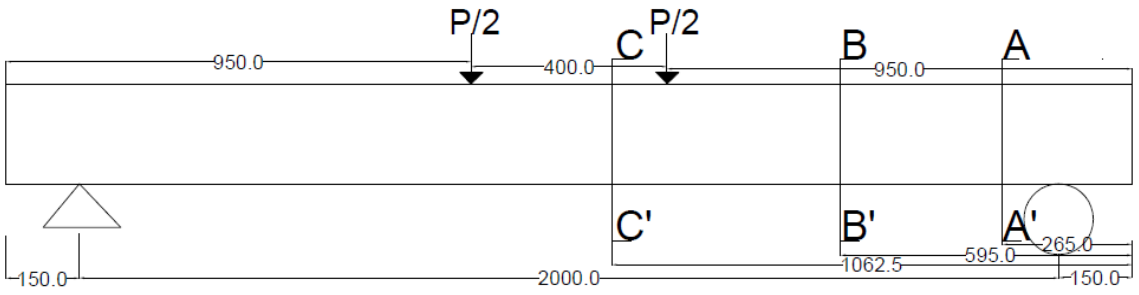

(a)

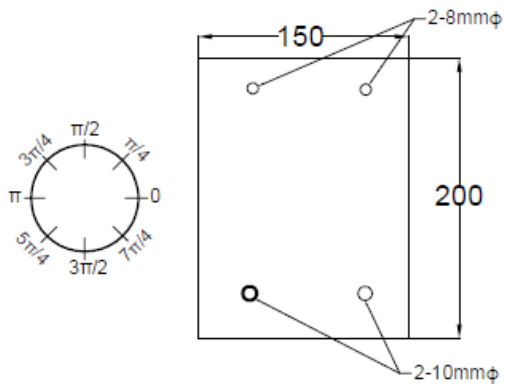

(b) **(c)**

Figure-4.21 (a) Location of section A-A', B-B' & C-C' on the RC beam of (b) Orientation of 10mmϕ bar (c) The selected interface on cross section of a beam for spalling stress

Figure-4.22 shows the contact pressure parameter at the rebar concrete interface due to corrosion of the bottom reinforcement. It represents the outward pressure at steel concrete interface. A highlighted interface in Figure-4.21c has selected to present variations of the spalling stress. Corroded beam type C2 is selected to observe the variations of spalling stresses at various sections along the length of the beam Figure-4.22. The bottom reinforcement bars of corroded beam C2 consist of 13.88% corrosion. Spalling stresses of 8.43 MPa were applied corresponding to 13.88% of corrosion at rebar and concrete interface. Initially, spalling stresses are applied in a way such that it remains constant for a particular level of rebar corrosion. However, bending stresses exist in the beam which upon increase, influence the contact pressure at steel and concrete interface. The experimental setup of the RC beam clearly indicates that bending moment developing in the RC beam at the sections A-A′, B-B′ and C-C′ are in ascending order. Significant variations of spalling stresses occur at a section which consists of the higher bending stress. Comparison of Figure- 4.22a, 4.22b and 4.22c establish that spalling stresses due to rebar corrosion vary with increase of bending stresses. To represent the variation at different damage level in the beam, three different loading conditions are chosen, which are cracking load, yield load and ultimate load. The spalling stresses are observed at the cross section of the rebar at all the three sections (A-A, B-B, and C-C) with increase of loading.

Figure-4.22 presents the contact pressure (MPa) around the rebar concrete interface at various sections. This contact pressure represents the spalling stresses around the interface. Interesting thing to notice that spalling stresses increases in the region up to cracking load and from yield load to ultimate load, whereas it reduces from cracking load to yield load as shown in Figure4.22a. Variation of spalling stresses with respect to bending stresses has not yet verified quantitatively. However, the variations of spalling stress explain the flexural cracking mechanism of the corroded RC beam. A decline of spalling stresses after cracking load describe as an effect due to flexural cracking in the RC beam. Flexural cracks on the RC beam generate once the load value crossed the cracking load of an RC beam. An RC beam release the energy due to development of flexural cracks and these flexural cracks are expected to reduce spalling pressure at rebar concrete interface. Although reduction in

stresses are different at different locations on the RC beam, Spalling stress variation in the flexural crack region of the corroded RC beam exhibit same type of trend. As we move towards support direction on the RC beam, the spalling stress observed to remain constant with increase of loading. At section B-B' in Figure-4.22b a different spalling stress scenario has been observed compared section A-A'. Spalling stresses are increased from cracking load to yield load and decreased from yield load to ultimate load. Section B-B' is located in between the loading point and support point as shown in Figure-4.21a. Hence, the development of cracking and yielding in that region legs compared to central part of the beam. Therefore, a shift has been observed in the spalling stress variations with decrease of bending stress along the length of the beam. At section A-A' spalling stress remains the constant because of negligible influence of bending stress.

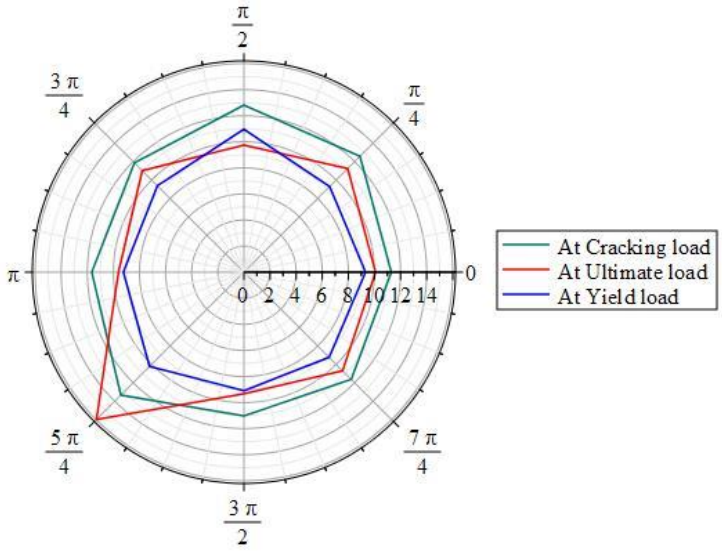

(a) Section C-C'

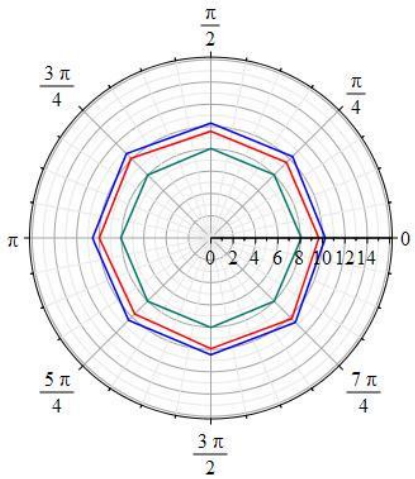

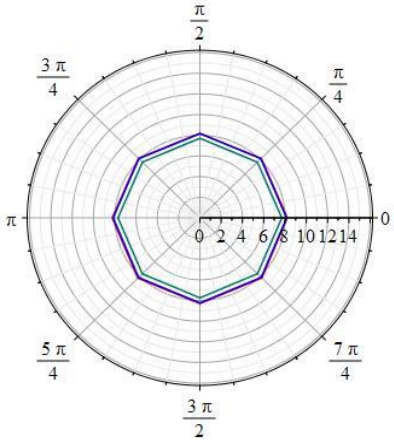

(b) Section B-B' **(c) Section A-A'**

Figure-4.22 Spalling stress distribution of C2 RC beam (a) section C-C' (b) section B-B' (c) section A-A'

The length of the RC beam can be divided into three zones 1) cracking zone 2) yielding zone and 3) post yielding zone based on flexural condition of the beam. Figure-4.23a, 4.23b and 4.23c present the flexural condition along the length of the beam at cracking load, yield load and ultimate load. Spalling stresses at steel concrete interface have observed to increase till cracking load, to decrease from cracking load to yield load.

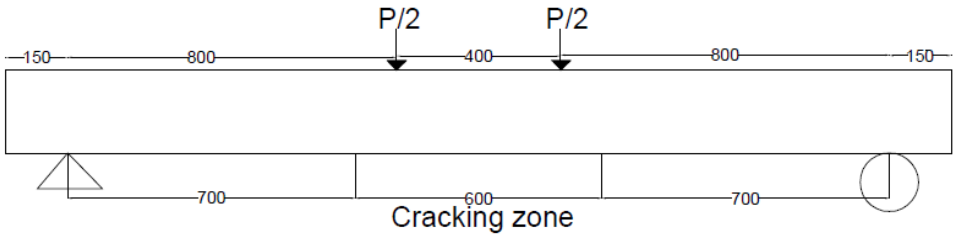

(a)

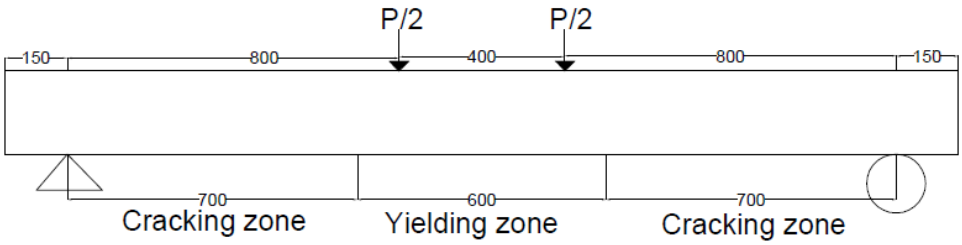

(b)

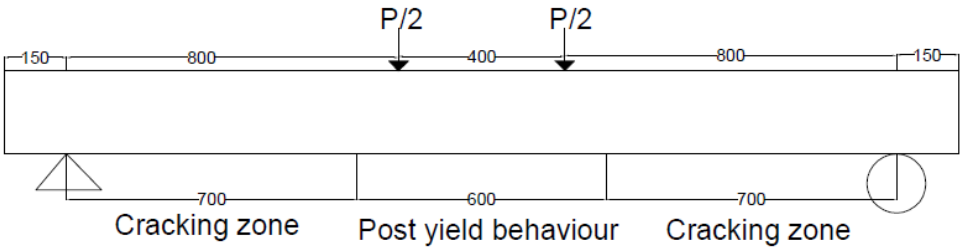

(c)

Figure-4.23 flexural behaviour along the length of the beam (a) At cracking load (b) At yield load (c) At ultimate load

Figure-4.24 shows the variation of spalling stress at 0^o node of the rebar cross section with respect to mid-span deflection and the length of the beam. The mid-span deflections corresponding to the cracking load, yield load and ultimate load of the beam are 2 mm, 9 mm and 25 mm, respectively. It is observed that at cracking load (2 mm deflection), the spalling stresses remain same along the length of the beam apart from central part of the beam. Since cracking initiates from the central region of the beam spalling stress increases in the central part of the beam. At yield load, (9 mm) spalling stress at central region is observed to decrease due to yielding while side regions (L/3 from each end) is experiencing the initiation of cracking. Hence spalling stress increases at the side region of the beam at 9 mm deflection. At a deflection of 25 mm, spalling stress varies at the central region of the beam, but it remains constant for end regions of the beam. It can be possibly because the end regions of the beam do not reach its yield point, while the central part of the beam has already crossed its yield point. Spalling stress increase at ultimate load at central part of the beam represent the post yield behaviour for corroded RC beam.

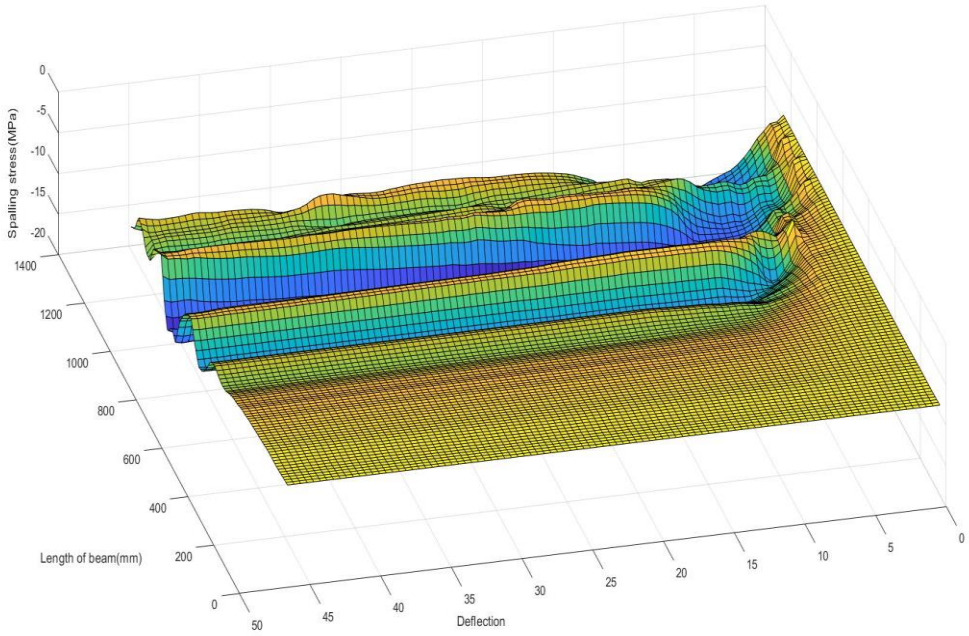

Figure-4.24 Spalling stress variation on 0^o node of the section C-C'

Figure - 4.25a and 4.25b present the spalling stresses around tensile reinforcement of beam type C1. The tensile reinforcement bars of C1 RC beam consist of 17.2% corrosion. Spalling stresses of 10.84 MPa were applied for 17.2% of corrosion at rebar concrete interface. Although spalling stresses value increase from C2 RC beam. It has been observed that the spalling stress variations is reduced with increase of rebar corrosion. Figure-4.26 presents the spalling stresses around tensile reinforcement bar of 26.04% corrosion. By comparing Figure-4.22a, 4.25a and 4.26a it has been noticed that with increase of corrosion spalling stress is increase. However, variation in the spalling stress is reduced. (Coronelli and Gambarova, 2004) reported that with increase of corrosion level in the reinforcement flexural cracks in the RC beam reduces and leads to brittle failure of the RC beam. The same phenomenon is also able to explain the reduction in the spalling stress variation. It has been noticed that spalling stress variation at section B-B' does not demonstrate any effect of increase in the corrosion level.

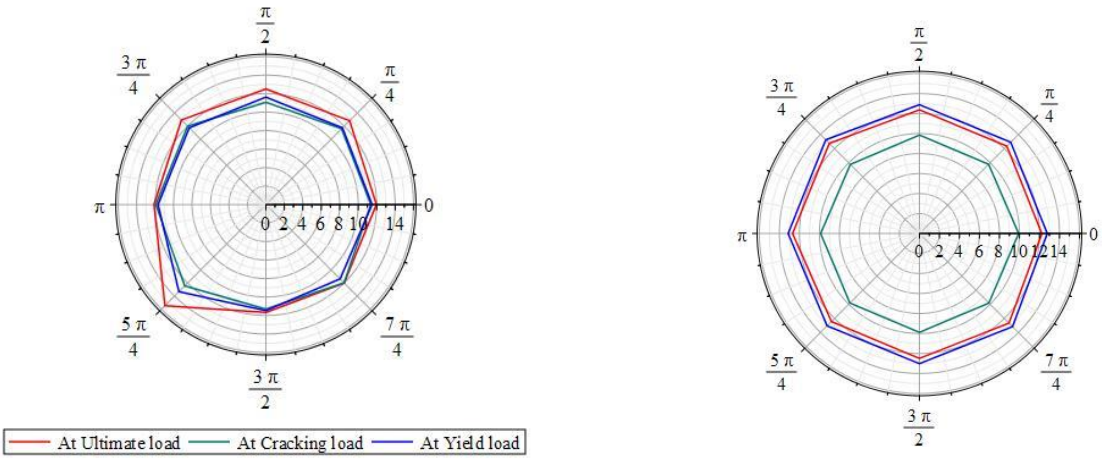

(a) **(b)**

Figure-4.25 Distribution of spalling stress for C1 RC beam at (a) section C-C' (b) section B-B'

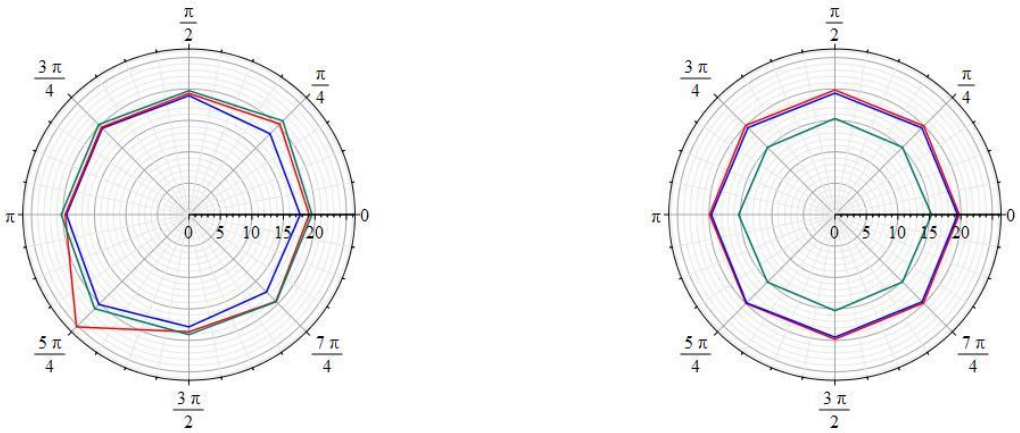

(a) **(b)**

Figure-4.26 Distribution of spalling stress for C3 RC beam at (a) Section C-C' (b) Section B-B'

4.3 EFFECT OF REBAR CORROSION UNDER SUSTAINABLE/DESIGN LOAD

In order to gain an insight on the evolution of damage due to corrosion, further FE analysis of (Lee *et al.*, 1999) RC beam is performed for various level of corrosion from 0% to 28% as shown in Figure-4.27. Numerical analyses for various corrosion level provide information about the performance of the RC beam at a constant service load. Evolution of load-deflection curve with the increase of corrosion level is observed to quantify the damage due to corrosion and to decide effective maintenance/repair strategy. Effect of corrosion at important points e.g. yield point, ultimate load point and ultimate deflection point of a load-deflection curve are studied to note their reduction compared to the control beam. In addition, the effect of sustainable loading on the corroded RC beam is noticed to make a better decision regarding the structural health maintenance or repair schedule of corroded RC beams.

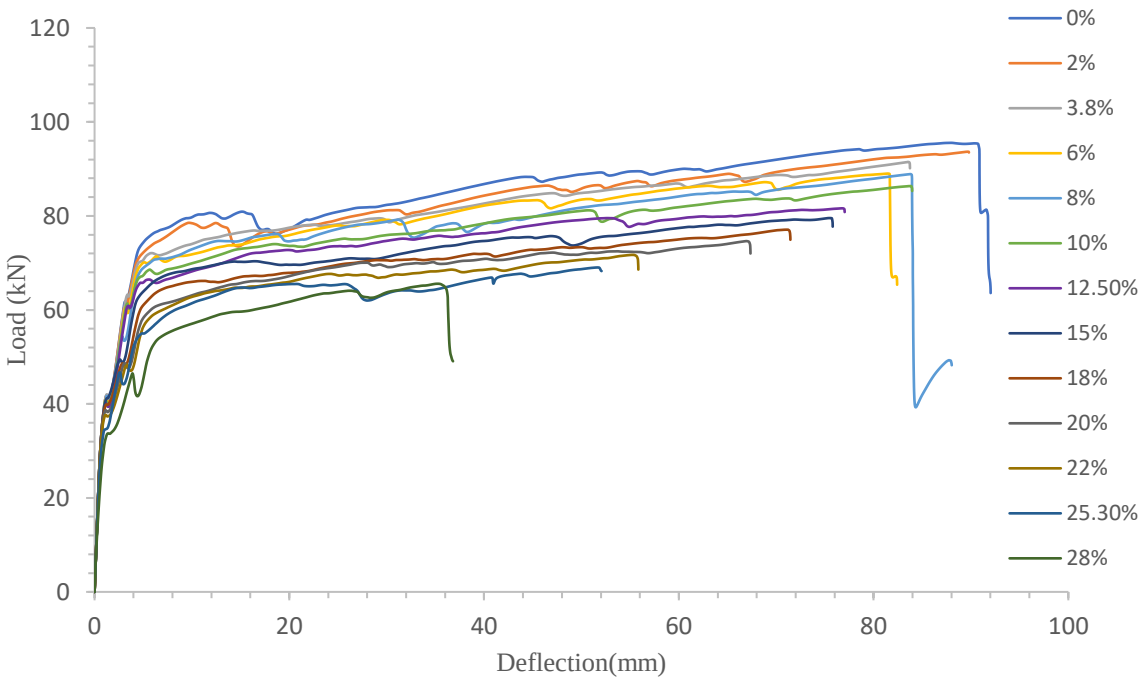

Figure-4.27 Load vs displacement curve at various level of corrosion

Reduction of load carrying capacity, yield load and ultimate deflection with the increase of corrosion level are presented in Table-4.6. A comparative study was done to observe the effect of corrosion on yield point, ultimate load point and the ultimate displacement point of the RC beam. The percentage reduction in the yield load, ultimate load and ultimate displacement obtained with respect to the values of control RC beam respectively.

Table -4.6 Reduction of yield load, ultimate load and ultimate deflection

Sr.No.	Corrosion (%)	Yield load (kN)	% Reduction	Ultimate load (kN)	% Reduction	Ultimate displacement (mm)	% Reduction
1	0	74.40	0	94.58	0	90.77	0
2	2	72.23	2.92	93.53	1.11	89.55	1.344
3	3.8	71.11	4.03	90.5	4.31	83.74	7.74
4	6	69.9	4.25	88.76	6.153	81.66	10.03
5	7.9	68.67	6.9	88.26	6.68	83.94	7.52
6	10	66.68	11	85.57	9.526	83.95	7.51
7	12.5	65.36	14.69	81.62	13.702	77.03	15.14
8	15	62.14	17.41	78.37	17.13	75.79	16.5
9	18	57.83	20.3	77	18.59	71.45	21.28
10	20	56.26	24.07	74.63	21.09	67.31	25.84
11	22	55.17	26.75	71.7	24.19	55.79	38.53
12	25.3	54.55	30.24	68.26	27.83	52	42.71
13	28	52.29	32.12	65.23	31.03	35.77	60.59

The percentage reduction of yield load, ultimate load and ultimate deflection with respect to different level of corrosion is shown in Figure-4.18. It is observed that the change or reduction in the yield load and ultimate load parameters vary almost linearly with level of corrosion (%) reaching up to a maximum value of 32% for a corrosion level of 28%. It is however interesting to note that the for a corrosion level of 28%, the reduction in the ultimate displacement with respect to the control beam is nearly 60%, which is very high compared to the yield or ultimate load. Although % reduction plot varies with loading conditions, support conditions, properties of a RC beam etc., the comparative effect on yield load, ultimate load and ultimate deflection may remain same with the increase of corrosion. Reduction in the yield load and ultimate load remain same with the increase of corrosion. While reduction for ultimate deflection of a corroded RC beam will be higher at higher level of corrosion.

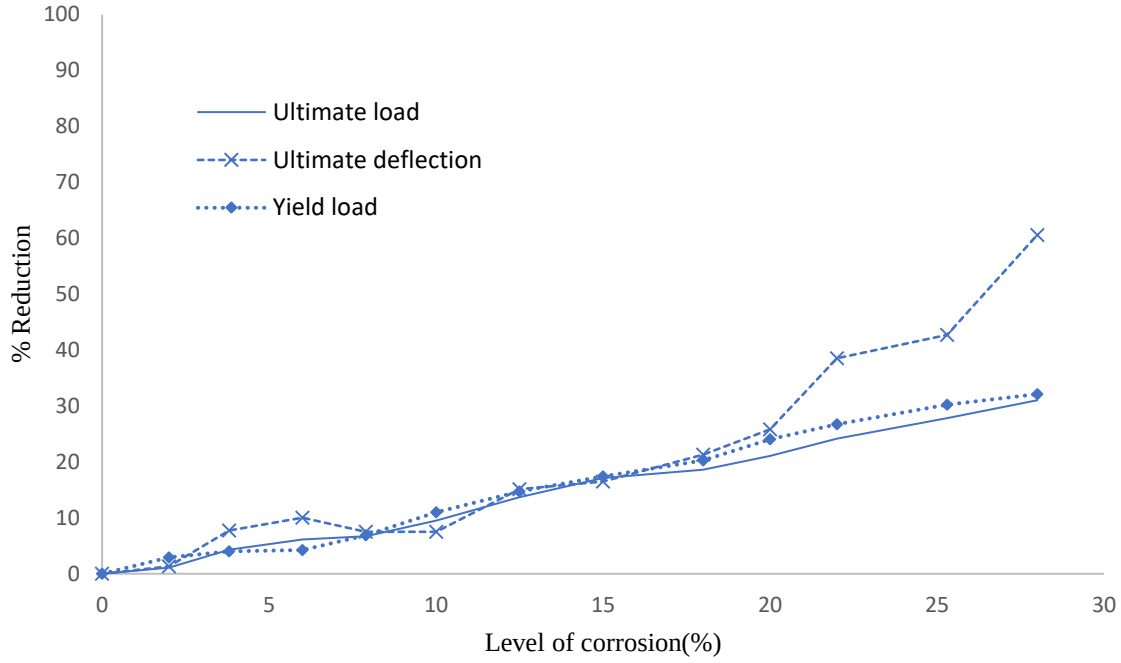

Figure-4.28 Percentage reduction in the yield load, ultimate load and ultimate displacement with respect to the level of corrosion (%)

The performance of the RC beam at a constant sustainable load and a design load has observed with a progressive increase of the corrosion level. As in real life situation, the corrosion level of rebars progressively increases while the RC beam resists the external loads. The moment carrying capacity of an RC beam describes as per Eq. (4.1) from IS:456-2000. The design load of the RC beam has calculated as 62 kN.

$$M_u = 0.87\, f_y\, A_{st} d \left(1 - \frac{A_{st} f_y}{f_{ck} b d}\right) \tag{4.1}$$

$$M_u = 0.87 \times 320 \times 398 \times 225 \left(1 - \frac{398 \times 320}{38 \times 200 \times 225}\right)$$

$$M_u = 23.07\ kNm$$

Design load $P = 2 \times \left(\frac{23.07}{0.75}\right)$

Design load $P = 62\ kN$

Limiting value of deflection for the RC beam calculated 8mm as per IS:456-2000. At a constant 62 kN load the deflection of various corroded RC beam is observed from the FE analysis results. The Figure-4.29a shows the variation of deflection with respect to % corrosion at 62 kN load. The plot provides deflection values up to 28% corrosion, as the further increase of corrosion level resulted in lower ultimate load values than 62 kN. Figure-4.29b shows the deflection of the RC beam with the increase of corrosion at 51 kN load. 51 kN load has considered as 82% of design load to notice the effect of corrosion on the serviceable load on the RC beam. By comparing both the curves of Figure-4.29a and 4.29b

it can be said that the maintenance/repair work schedule also depends on the RC beam loading apart from the level of corrosion in the RC beam.

At the 62 kN of loading of the RC beam, the rate of increase in the deflection value starts increasing rapidly from 15% corrosion. Further increase in the deflection of the RC beam will happen in a very less increase of corrosion level. Maintenance/repair cost of the RC beam will also increase parallel with the increase of the deflection. Therefore 15% corrosion level is the optimum maintenance point for the RC beam experiences 62 kN of the load. Interestingly, a huge difference in the % corrosion at the *optimum maintenance point* is observed when 51 kN load is considered (Fig 4.29b). A significant difference noticed in terms of the time frame of the optimum maintenance point between 62 kN load and 51 kN load. Along with Environmental factors, loading conditions on the RC beam also affect the maintenance/repair work strategy.

This scenario is very much likely to occur in bridges. Bridges used to design based on its predicted service load, however, an increased in the use of infrastructures and growth rate of the population lead to experience higher service loads than expected service loads on the bridges. Since at higher service loads the effect of rebar corrosion magnifies, the maintenance/repair work policy should also modify accordingly.

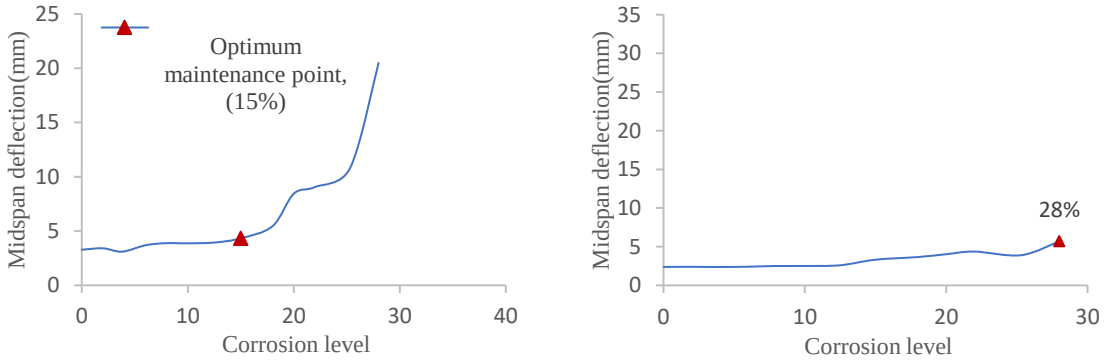

(a) **(b)**

Figure4.29 Deflection vs Corrosion level (%) (a) at design load 62 KN (b) at 51 KN load

A serviceability limit for deflection of the RC beam is 8 mm obtained from span/250 as per IS:456-2000. Further increase in the deflection of the RC beam makes the beam unserviceable. Figure-4.30 shows the load values obtained at 8 mm deflection of the RC beam for various level of corrosion (%). Since the design load for considered RC beam is 62 kN, structural capacity below 62 kN will not satisfy the serviceability criteria. The maximum allowable level of rebar corrosion (%) without any repair work on the RC beam is found to be 18% as shown in Figure-4.30.

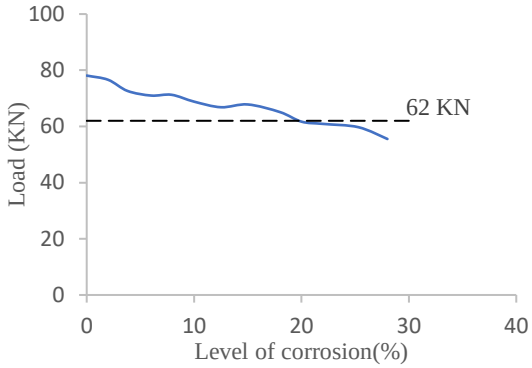

Figure-4.30 Load vs level of Corrosion (%) at allowable deflection of 8 mm

Displacement ductility index is evaluated based on the results of the finite element analysis. it is defined as the ratio of ultimate deflection to the deflection at the yield load as per Eq.-4.2. Figure-4.31 present the variation of the ductility index with respect to corrosion level. *Δu* and *Δy* are the deflection at ultimate load and yield load of the RC beam respectively.

$$\mu_u = \frac{\Delta u}{\Delta y} \tag{4.2}$$

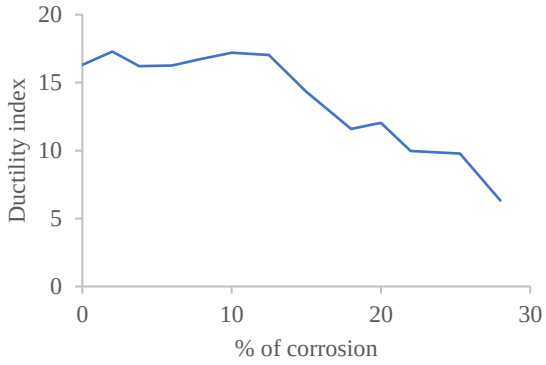

Figure -4.31 Ductility index vs level of corrosion (%)

CHAPTER-5

CONCLUSION

In the present study, the nonlinear response of corroded RC beams is obtained by the finite element analysis which includes the bond slip model and spalling stresses. The results of finite element analysis validated with experimental investigation of Rodriguez *et al.,* (1997) and Lee *et al.,* (1999). Spalling stress variation has presented with respect to length and midspan deflection of the beam. Optimum maintenance point has obtained for corroded RC beams to avoid excessive maintenance losses. The following salient conclusions have been found from the finite element analysis of corroded RC beams.

- The load carrying capacity and the ultimate deflection of the RC beam reduces with increase of corrosion level. Ultimate deflection point of a corroded RC beam depends on the spalling stress, bond strength and ultimate strain of rebars. The reduction in the ultimate deflection of a corroded RC beam accelerate at higher corrosion level around 20%. Neglecting the spalling stress effect for 25.3% corroded RC beam resulted into 29% lower ultimate deflection value of the corroded RC beam.
- Optimum maintenance point has found for an RC beam as 15% level of corrosion based on given boundary conditions and specifications. Increase in the service loads on an RC beam significantly reduces the time period for maintenance and repair work of a beam.
- Spalling stress due to rebar corrosion varies under the influence of bending stress of the RC beam. Flexural cracks region governs the spalling stress variation along the length of the RC beam. Increase of the corrosion level decreases the influence of bending stress as less variation in the spalling stress have observed at higher level of corrosion.

5.1 FUTURE SCOPE

The influence of bending stress on the variation of spalling stress require experimental investigation to establish quantitative relations. The influence of spalling stress, bond degradation and ultimate strain of rebars on the failure point of the RC beam has not yet studied extensively. An overall methodology is needed to establish in the design procedure of RC structures which include the effect of corrosion.

REFRENCES

ABAQUS 6.14 Documentation, Dassault Systèmes Simulia Corp., Providence,RI, USA.

Alfarah, B., López-Almansa, F. and Oller, S. (2017) 'New methodology for calculating damage variables evolution in Plastic Damage Model for RC structures', *Engineering Structures*. Elsevier Ltd, 132, 70–86. doi: 10.1016/j.engstruct.2016.11.022.

Bhargava, K. *et al.* (2007) 'Corrosion-induced bond strength degradation in reinforced concrete-Analytical and empirical models', *Nuclear Engineering and Design*, 237(11), 1140–1157. doi: 10.1016/j.nucengdes.2007.01.010.

Bhargava, K. *et al.* (2008) 'Suggested Empirical Models for Corrosion-Induced Bond', 134, 221–230.

Biondini, F. and Vergani, M. (2014) 'Deteriorating beam finite element for nonlinear analysis of concrete structures under corrosion'. Taylor & Francis, 2479. doi: 10.1080/15732479.2014.951863.

Broomfield J.P. (2007) *Corrosion of steel in concrete: Understanding, investigation and repair, 2nd Ed., Taylor and Francis, U*.

Cabrera, J. G. (1996) 'Deterioration of concrete due to reinforcement steel corrosion', *Cement and Concrete Composites*, 18(1), 47–59. doi: 10.1016/0958-9465(95)00043-7.

Castel, A. and François, R.; Arliguie, G. (2000) 'Mechanical behaviour of corroded reinforced concrete beams—Part 2: Bond and notch effects', *Materials and Structures*, 33(9), 545–551.

CEB-FIP (2010) *Model Code 2010, fib Model Code for Concrete Structures 2010*. doi: 10.1002/9783433604090.ch6.

Chung, L. *et al.* (2004) 'Correction factor suggestion for ACI development length provisions based on flexural testing of RC slabs with various levels of corroded reinforcing bars', *Engineering Structures*, 26(8), 1013–1026. doi: 10.1016/j.engstruct.2004.01.008.

Committee on the safety of nuclear Installations (2002) 'NEA / CSNI / R (2002) 21 Unclassified'.

Coronelli, D. and Gambarova, P. (2004) 'Structural Assessment of Corroded Reinforced Concrete Beams : Modeling Guidelines', 130(8), 1214–1224.

Dekoster, M. *et al.* (2003) ‘Modelling of the flexural behaviour of RC beams subjected to localised and uniform corrosion’, *Engineering Structures*, 25(10), 1333–1341. doi: 10.1016/S0141-0296(03)00108-1.

Grassl, P. and Jirásek, M. (2006) ‘Damage-plastic model for concrete failure’, *International Journal of Solids and Structures*, 43(22–23), 7166–7196. doi: 10.1016/j.ijsolstr.2006.06.032.

Hordijk, D. A. (1992) 'Tensile and tensile fatigue behaviour of concrete; experiments, modelling and analyses'. *Heron*, *37*(1).

Jiang, C., Wu, Y. F. and Dai, M. J. (2018) ‘Degradation of steel-to-concrete bond due to corrosion’, *Construction and Building Materials*. Elsevier Ltd, 158, 1073–1080. doi: 10.1016/j.conbuildmat.2017.09.142.

Kamaitis, Z. (2011) ‘Damage to concrete bridges due to reinforcement corrosion. part i. site investigations’, 17(4), 137–142. doi: 10.1080/16483840.2002.10414030.

Lee, H. . *et al.* (1999) ‘The Evaluation of Flexural Strength of RC Beams’, 321–330.

Lee, H. S., Noguchi, T. and Tomosawa, F. (2002) ‘Evaluation of the bond properties between concrete and reinforcement as a function of the degree of reinforcement corrosion’, *Cement and Concrete Research*, 32(8), 1313–1318. doi: 10.1016/S0008-8846(02)00783-4.

Lin, H. *et al.* (2017) ‘Bond strength evaluation of corroded steel bars via the surface crack width induced by reinforcement corrosion’, *Engineering Structures*, 152, 506–522. doi: 10.1016/j.engstruct.2017.08.051.

Liu Y and Wayers R. (1998) 'Modeling the time to corrosion cracking in choride contaminated reinforced concrete structures'. ACI Material Journal, 95(6), 675-681

El Maaddawy, A. T. and Soudki, A. K. (2003) ‘Effectiveness of Impressed Current Technique to Simulate Corrosion of Steel Reinforcement in Concrete’, *Journal of Materials in Civil Engineering*, 15(1), 41–47. doi: 10.1061/(ASCE)0899-1561(2003)15:1(41).

Maaddawy, E., Soudki, K. and Topper, T. (2006) ‘Long-term performance of corrosion-damaged reinforced concrete beams’, *ACI stractural Journal*, 102(5), 649–656.

El Maaddawy, T. and Soudki, K. (2007) ‘A model for prediction of time from corrosion initiation to corrosion cracking’, *Cement and Concrete Composites*, 29(3), 168–175. doi: 10.1016/j.cemconcomp.2006.11.004.

Otieno, M. B., Beushausen, H. D. and Alexander, M. G. (2011) 'Modelling corrosion propagation in reinforced concrete structures - A critical review', *Cement and Concrete Composites*. Elsevier Ltd, 33(2), 240–245. doi: 10.1016/j.cemconcomp.2010.11.002.

Ožbolt, J., Balabanić, G. and Kušter, M. (2011) '3D Numerical modelling of steel corrosion in concrete structures', *Corrosion Science*, 53(12), 4166–4177. doi: 10.1016/j.corsci.2011.08.026.

Rodriguez, J., Ortega, L. M. and Casal, J. (1997) 'Load Carrying Capacity of Concrete Structures With', *Construction and Building Materials*, 11(4), 239–248.

Sharma, S. and Mukherjee, A. (2011) 'Monitoring corrosion in oxide and chloride environments using ultrasonic guided waves', *Journal of Materials in Civil Engineering*, 23(2), 207–211. doi: 10.1061/(ASCE)MT.1943-5533.0000144.

Torres-Acosta, A. A., Navarro-Gutierrez, S. and Terán-Guillén, J. (2007) 'Residual flexure capacity of corroded reinforced concrete beams', *Engineering Structures*, 29(6), 1145–1152. doi: 10.1016/j.engstruct.2006.07.018.

Yu, L. *et al.* (2015) 'Structural performance of RC beams damaged by natural corrosion under sustained loading in a chloride environment', *Engineering Structures*. Elsevier Ltd, 96, 30–40. doi: 10.1016/j.engstruct.2015.04.001.